Volume 16 | Number 10 | 21 May 2016 | Pages 1711–1948

Lab on a Chip

Miniaturisation for chemistry, physics, biology, materials science and bioengineering

www.rsc.org/loc

ISSN 1473-0197

ROYAL SOCIETY OF CHEMISTRY

CRITICAL REVIEW
Albert Folch *et al.*
The upcoming 3D-printing revolution in microfluidics

175 YEARS

Lab on a Chip

CRITICAL REVIEW

View Article Online
View Journal | View Issue

Cite this: *Lab Chip*, 2016, **16**, 1720

The upcoming 3D-printing revolution in microfluidics

Nirveek Bhattacharjee,[a] Arturo Urrios,[ab] Shawn Kang[a] and Albert Folch*[a]

Received 4th February 2016,
Accepted 1st April 2016

DOI: 10.1039/c6lc00163g

www.rsc.org/loc

In the last two decades, the vast majority of microfluidic systems have been built in poly(dimethylsiloxane) (PDMS) by soft lithography, a technique based on PDMS micromolding. A long list of key PDMS properties have contributed to the success of soft lithography: PDMS is biocompatible, elastomeric, transparent, gas-permeable, water-impermeable, fairly inexpensive, copyright-free, and rapidly prototyped with high precision using simple procedures. However, the fabrication process typically involves substantial human labor, which tends to make PDMS devices difficult to disseminate outside of research labs, and the layered molding limits the 3D complexity of the devices that can be produced. 3D-printing has recently attracted attention as a way to fabricate microfluidic systems due to its automated, assembly-free 3D fabrication, rapidly decreasing costs, and fast-improving resolution and throughput. Resins with properties approaching those of PDMS are being developed. Here we review past and recent efforts in 3D-printing of microfluidic systems. We compare the salient features of PDMS molding with those of 3D-printing and we give an overview of the critical barriers that have prevented the adoption of 3D-printing by microfluidic developers, namely resolution, throughput, and resin biocompatibility. We also evaluate the various forces that are persuading researchers to abandon PDMS molding in favor of 3D-printing in growing numbers.

1. The manufacturability roadblock

Microfluidic device fabrication is presently dominated by molding approaches based on poly(dimethylsiloxane) (PDMS) and thermoplastics.[1,2] However, with an increasing focus on translation and low-cost devices, these approaches are facing a "manufacturability roadblock". Manufacturability should not be confused with high-throughput fabrication. A device is easily manufacturable when it can be brought to market at a low cost (including resources and development) using a reliable process.[3] Unfortunately, it is very difficult for an engineer to disseminate his/her PDMS device(s) to a community of biomedical scientists. Three major challenges have so far hindered the commercialization of PDMS chips: 1) PDMS molding (including PDMS curing, assembly, bonding, and inlet punching) is a largely manual process, being hard to fully automate – which means that fabrication is expensive and PDMS-molded devices cannot possibly meet the vision of inexpensive, batch-fabricated MEMS devices; 2) for many years, the user interfaces (inlets/outlets) of PDMS chips have consisted of punched or molded holes that are prone to leakage and are awkward to connect – as opposed to the leak-free, intuitive connectors such as the industry-standard Luer-lock, barbed connectors, *etc.* that doctors and biologists are used to working with; and 3) the control systems required to run microfluidic valves (ranging from the computer, pressure sources, software, *etc.*), or even to connect relatively simple chips, involve engineering expertise and equipment not present in most biomedical laboratories.

Devices molded in thermoplastics (*e.g.* polystyrene, PMMA, polyurethane, *etc.*) enable higher throughput, but do not necessarily allow superior manufacturability. Another problem with thermoplastics is that since the Young's modulus of hard plastics is typically three orders of magnitude larger than that of PDMS, any flexural element made of hard plastic will bend ~1000 times less than PDMS so it will need to be built larger to achieve similar deflections. In addition, bigger valves have lower cutoff frequencies, so PDMS valves will always outperform plastic valves of similar size. Veres and co-workers have pioneered the use of thermoplastic elastomers (TPE), mainly styrene-(ethylene/butylene)-styrene block co-polymer (SEBS), as an alternative to PDMS for high-throughput microfluidic fabrication.[4] However, the academic community has been reluctant to work with thermoplastics and injection molding because they are not amenable to rapid-prototyping: both the equipment and the molds are expensive, the turn-around times for the fabrication of the

[a] *Department of Bioengineering, University of Washington, Seattle, Washington, USA. E-mail: afolch@uw.edu*
[b] *Cell Signaling Research Group, Departament de Ciències Experimentals i de la Salut, Universitat Pompeu Fabra (UPF), E-08003 Barcelona, Spain*

metallic molds can be on the order of weeks (*e.g.* ProtoLabs offers parts in "less than 3 weeks"), and the molding procedure requires substantial expertise. Everyone cannot afford such an investment in resources and time. Cheaper, more user-friendly forms of plastic molding exist (*e.g.* thermoforming[5] or hot embossing[1,6]), but with lower throughputs, less resolution, challenges in valve fabrication, and identical constraints of bonding and layered design as PDMS molding.

Starting a microfluidics company that produces a molded device requires very large investments. More than two decades after the foundational paper by Andreas Manz and coworkers that announced the birth of the "Total Analysis Systems",[7] the number of companies that have successfully commercialized a microfluidic device is dismally low, with Fluidigm being the notable exception. While Fluidigm, indeed, has had an enormous impact in areas such as genomics, biophysics and biochemistry, the high cost of its chips and the large size of the investments raises serious doubts about whether most microfluidics startups can afford to produce their chips by PDMS or thermoplastic molding.

In the last ten years, NIH launched a massive "translational" effort to stimulate engineers into thinking about how to bring their inventions to market, and it soon started bearing manufacturable fruits. In 2008, George Whitesides' group proposed a creative solution to both the problem of cost and to the requirement of pumps: make the devices in paper.[8] Paper is an inexpensive material, it self-pumps the fluids with its wicking action, and it can be patterned for pennies in any office with a simple wax printer. The field took a new turn because the technology suddenly was able to reach new communities – not only biomedical laboratories, but also disfavored communities in distant countries. The problem is that the wicking action of paper cannot be stopped (some contraptions have been invented, but the cost will no longer be as low), and paper is not a good medium for cell manipulation, so even a relatively simple, but biotechnologically important, cell sorting assay seems to face unsurmountable challenges in the paper format.

In order to maximize manufacturability (and impact), it is essential to minimize total cost. We would like devices made of a material that can be rapidly prototyped (like PDMS or paper), manufactured for low cost per unit (like paper or injection molding), and where laminar flow can also be controlled, stopped, and re-started with negligible energy consumption and minimal expertise requirements – so that we can bring, for example, an automated, autonomous cancer cell sorting assay to rural towns. Here we show many examples leading us to believe that 3D-printing is the technology that will allow researchers to dodge the roadblock. 3D-printing does not aim to substitute injection-molding as a 3D-printer is unlikely to be able to produce tens of thousands of parts per day. 3D-printing is a rapid-prototyping, 3D digital manufacturing process that affords production of small batches of parts while allowing for a smooth transition to injection-molding for those applications that demand high-throughput production.

2. 3D-printed microfluidic systems come in different flavors

"3D-printing" refers to a set of additive manufacturing techniques, which can create solid three-dimensional (3D) objects layer-by-layer under precise digital control. Of these techniques, the ones that are most relevant to microfluidic device fabrication are (a) stereolithography (SL) (Fig. 1A), (b) multi jet modeling (MJM) (Fig. 1B) and (c) fused deposition modeling (FDM) (Fig. 1C). Selective laser sintering (SLS) is another rapid prototyping technique widely used for superior prototype design in manufacturing industries. SLS has a diverse range of biomedical applications, particularly in building scaffolds for bone tissue engineering, surgical models of organs, personalized prosthetics and implants, and

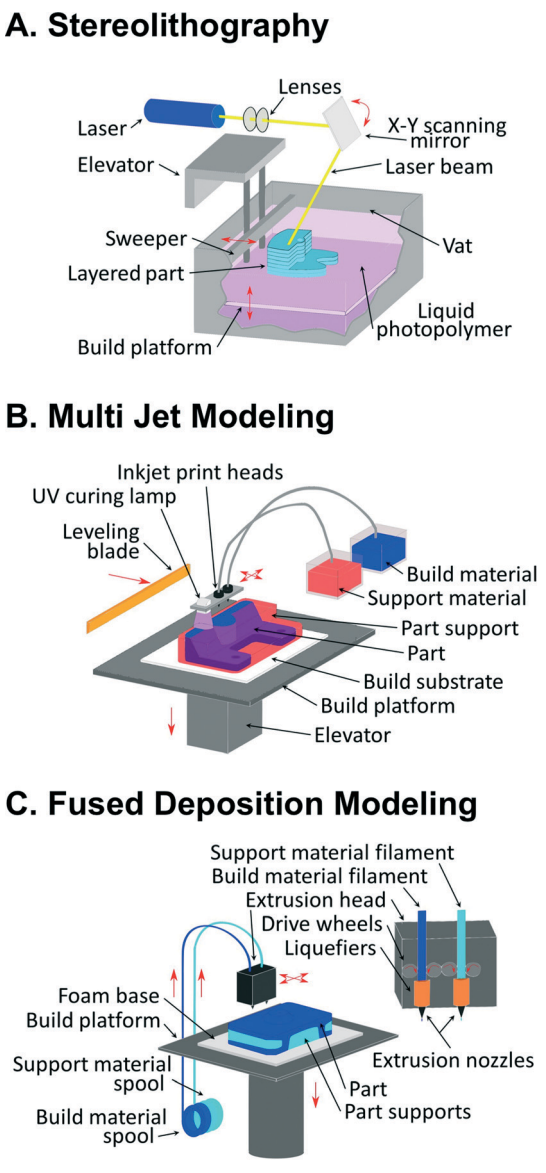

Fig. 1 Various 3D-printing techniques. (A) Stereolithography (SL); (B) multi jet modeling (MJM); (C) fused deposition modeling (FDM), also termed "thermoplastic extrusion".

biodegradable drug-delivery devices.[9–11] However, since SLS is unsuitable for making microfluidic devices (the powder precursor is very difficult to remove from small cavities), we do not cover it in this review.

2.A. By stereolithography (SL)

Stereolithography (SL) is a form of 3D printing invented in the 1980s that allows for the assembly-free production of quasi-arbitrary 3D shapes in a single polymeric material from a photoresin precursor by means of a focused laser or LED light source.[12] While the initial invention by Hull utilized only material that could be cured by UV, recent advances in laser technology and photochemistry of resins have enabled polymerization of photoresins with high-intensity and focused LED light sources in the visible wavelength.[13] The minimum feature size (resolution) that is achievable by traditional SL is dependent on the laser spot size and the absorption spectra of the photoresins.[14]

A more recently developed strategy uses digital light projection (DLP) to expose an entire layer of resin at once (first shown using a liquid crystal display (LCD)[15]). In DLP-based SL, the resolution is determined by the size of the projected pixel. With the advent of inexpensive digital micromirror display (DMD) technology and commercially available projectors, the cost of DLP printers has come down significantly.[16]

In SL, a 3D object is built layer-by-layer by using selective light exposure to photo-polymerize a precursor resin collected in a vat. Each layer is projected as an image obtained by digitally sectioning the 3D object into thin slices. The surface along which the photo-polymerization of the resin takes place broadly differentiates SL into two approaches[17] (Fig. 2). In the "free surface" approach, used by the earlier SL machines designed by 3D Systems, the resin is photo-polymerized by a laser at its topmost surface that interfaces with air. In this configuration, the metal build stage is always submerged in the resin vat and is translated downwards into the vat after every layer is printed (Fig. 2A). On the other hand, the more recent laser-based and all the DLP systems use the "constrained surface" approach, where the resin is photo-polymerized against the bottom surface of the vat. In this approach, the metal build plate, suspended upside down above the vat, is brought down into the resin vat for the building of a layer by photo-polymerization, and is then separated from the bottom-surface of the vat (that is usually coated by PDMS for easy separation) and returned to the original suspended position. This configuration results in the building of the final object in an upside-down orientation, and is therefore commonly referred to as the "bat" configuration[13] (Fig. 2B).

Both these approaches have their advantages and drawbacks. The structural fidelity is superior in the free surface technique over the constrained surface technique, as the mechanical separation step of the bat configuration can induce stress fractures or bending of delicate features and increase roughness between layers. However, in the free surface technique, the vat depth limits the object height, whereas in the bat configuration, there is no such limitation. Furthermore, since oxygen inhibits the process of photo-polymerization, the time of curing is faster in the bat configuration, where the reaction happens away from the air-resin interface. Some recent modifications to the constrained surface technique make the bottom plate permeable to oxygen and utilize controlled oxygen inhibition to prevent the most recently cured resin layer from adhering to the bottom plate. Since the last photo-polymerized region remains suspended in the resin, separating the bottom plate from the built part is no longer

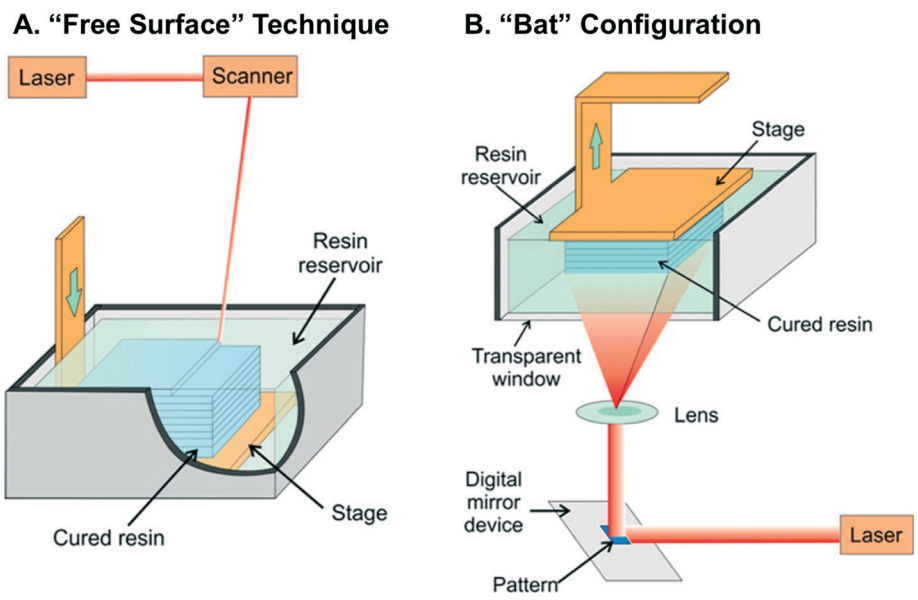

Fig. 2 SL configurations. (A) "free surface" SL technique; (B) "constrained surface" SL technique or the "bat" configuration SL printing. Panels (A) and (B) are reproduced from ref. 17 with permission of the American Chemical Society.

needed at every step. The printing speeds can therefore be increased almost 100 times in this "continuous printing" approach.[18]

In SL, a microchannel is built by photo-polymerizing the channel walls and then draining the uncured resin from the channel cavity, after the printing is complete.[19] Fig. 3 shows a few microfluidic devices built with SL. In 2000, Renaud's group presented the first SL-printed microfluidic device – a microfluidic mixer with an arrangement of rigid elements that enables superior mixing by splitting, combining and rearranging the flow-lines[20] (Fig. 3A). Such an intricate 3D inner architecture, that fully and efficiently mixed fluids (at Re = 12) within 4 mm, was not possible with molding and layering.[21] DMD-based SL has been used to create hollow, ~1 mm long micro-needles (with a bore diameter of 375 μm) that could penetrate cadaveric porcine skin[22] (Fig. 3B). Lately, microfluidic devices for immunomagnetic separation of bacteria,[23] separation of cells by using helical channels with trapezoid cross-sections[24] (Fig. 3C), gradient generation[25] (Fig. 3D), emulsion droplet generators,[25–28] DNA assembly[29] and an oxygen control insert for a 24-well dish,[30] to name a few, have been designed using single-photon SL. The minimum cross-sectional area of a microchannel that is attainable by SL depends not only on the laser spot-size or pixel resolution, but also on the type and viscosity of the resin, which has to be effectively drained from the channels post-printing.[31]

Employing multi-photon optics can increase the resolution of 3D fabrication to sub-micron levels by tightly focussing high-intensity pulsed laser beams to femtoliter volumes.[32–34] In multi-photon direct laser writing, the photosensitive group in a polymer matrix gets excited by absorbing two (or more) photons simultaneously, which can take place only in volumes that has the highest photon flux.[35] The *N*-photon absorption rate is a *N*th order process and steeply decreases with distance from the focal plane.[35] Very high-resolution 3D structures can be printed with DLW by moving the tightly focussed laser beams in the 3D space. However, the speed of writing is very slow (in the order of mm s^{-1}),[32] and DLW systems are very expensive. Multiphoton 3D fabrication has been used to create high-resolution 3D protein micro-structures,[36] which have been used as "lobster-traps" for bacterial cells[37] (Fig. 3E–F) or to capture bacteria and harness its flagellar motion to drive microfluidic flow.[38] While DLW can be used to fabricate complex and arbitrary 3D structures, it does not belong to the class of additive manufacturing techniques that build 3D structures layer-by-layer because it requires dissolution of material (subtractive processing). Therefore, we do not cover DLW in detail here (see recent reviews on DLW[32,35] and its applications in microfluidics[39]).

2.B. By multi jet modeling (photopolymer inkjet printing)

Multi jet modeling (MJM) is a form of 3D printing where each layer is built onto a tray *via* an inkjet head, which delivers curable liquid photopolymer that is rapidly polymerized by UV. In cases where overhanging structures or complex shapes require

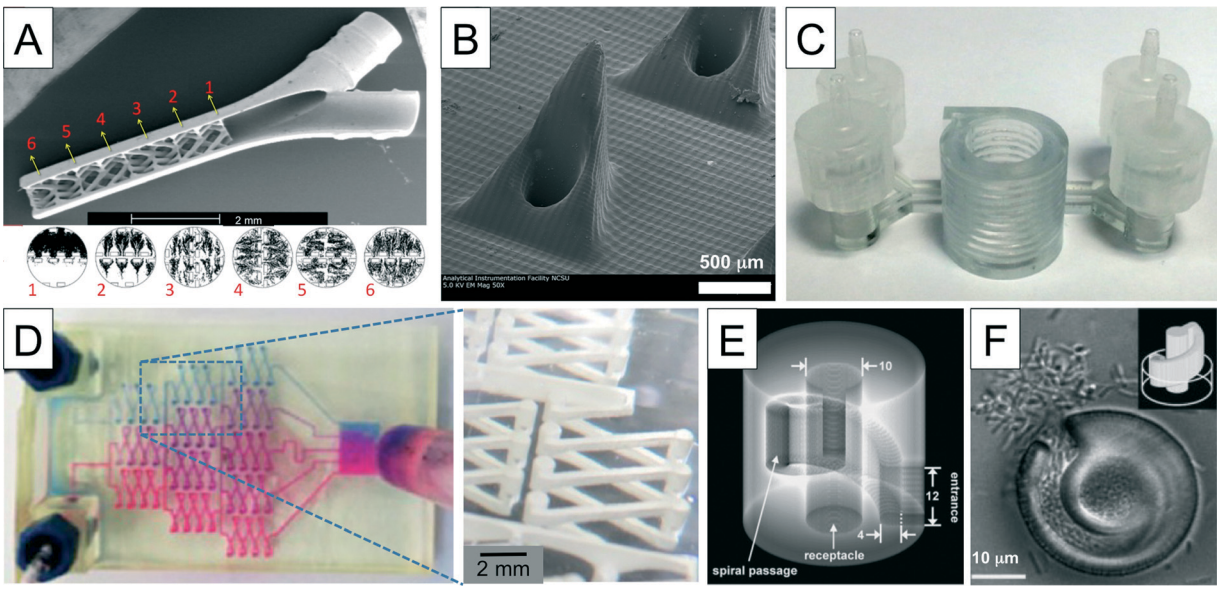

Fig. 3 Microfluidic devices printed with SL. (A) SEM micrograph of the first microfluidic device (micro-mixer) printed with SL. (below) numerical simulations of fluid mixing at the indicated cross-sections of the device. (B) SEM of hollow micro-needles fabricated in e-Shell-200 by DLP-SL. (C) Spiral microchannel with trapezoid cross-section (printed with Watershed) used for size-selective separation of bacterial cells. (D) A complex microfluidic mixer and gradient generator printed with a commercial desktop SL system. (E) A microfluidic "lobster trap" for bacteria fabricated in bovine serum albumin with multi-photon SL. (F) A colony of *E. coli* forming at the bottom of the "lobster trap". Panel (A) is reproduced from ref. 20 with permission of the Royal Society of Chemistry. Panel (B) is reproduced from ref. 22 with permission of the American Institute of Physics. Panel (C) is reproduced from ref. 24 under the Creative Commons Attribution-non Commercial-noderivs 4.0 International License. Panel (D) is reproduced from ref. 25 with permission of the American Chemical Society. Panels (E) and (F) are reproduced from ref. 37 with permission of John Wiley and Sons.

support, the inkjets can deliver a gel-like sacrificial material that may be dissolved after the build is complete. Patented in 1999 by Objet, a company later acquired by Stratasys, this printing method is also known as "Polyjet" or "Photopolymer Inkjet Printing". In a similar 3D printing technique called "Binder Jetting", an inkjet head dispenses a mixture of an aqueous binding agent and a powder instead of the proprietary Objet/Stratasys inks to create 3D objects layer by layer; the powder itself acts as the support or sacrificial material.

One of the greatest advantages of MJM printing is that the inkjets can deliver multiple materials at the same time to build an object, with a wide range of material properties (hard and soft plastics, elastomers) and different colors.[40] However the material formulations used in MJM printers are proprietary and expensive, and rigorous biocompatibility and biofunctionality studies are absent so far. MJM technology has been widely used in the medical sector to create anatomically accurate models for orthopedic,[41] cardiac[42] and intracranial[43] surgeries. Both MJM and binder jet methods can build structures that are comparatively large (8 inch cube), and have been used to build prototypes with smooth finishes and complex shapes, including manufacturing tools, working gears and metallic electrodes.[44]

MJM printing is an attractive technology for microfluidic applications, because of its high resolution and multi-material printing capability. However a sacrificial material that can be reliably cleared from an enclosed channel is key to producing arbitrary microfluidic channel networks in a single step by MJM printing. Fig. 4 shows some of the microfluidic devices that have been printed with MJM. Linear microchannels up to 500 μm in diameter, where the internal cavity is cleared by a cylindrical probe, or sonication and compressed air, have been built with VeroClear (an acrylate-based material, from Stratasys).[45] MJM-printed flow channels have been integrated with porous semi-permeable membranes supporting cell culture, to study transport and pharmacokinetic profiling of drugs[46,47] (Fig. 4A). A soluble support dissolvable with NaOH has been recently released by Stratasys under the trade-name SUP706. This option might be better for creating smaller microchannels, but the removal step is limited by diffusion and still quite challenging. Recently, Sochol *et al.* used a Projet printer to print integrated fluidic circuits, having both static and dynamic elements, with VisiJet M3 Crystal as the photo-curable plastic and wax as the sacrificial resin. After printing, the wax was cleared by first heating the entire printed block to 80 °C and then sequentially flowing hot mineral oil and compressed air through the internal channel voids, whose smallest dimensions were ~200 μm. "Bellow-diaphragms" that were 1–2 cm in diameter and 150 μm in thickness served as the dynamic deformable element and were used in designing fluidic capacitors, diodes, transistors and a multi-flow controller device[48] (Fig. 4B). A microfluidic mixer and homogenizer[49]

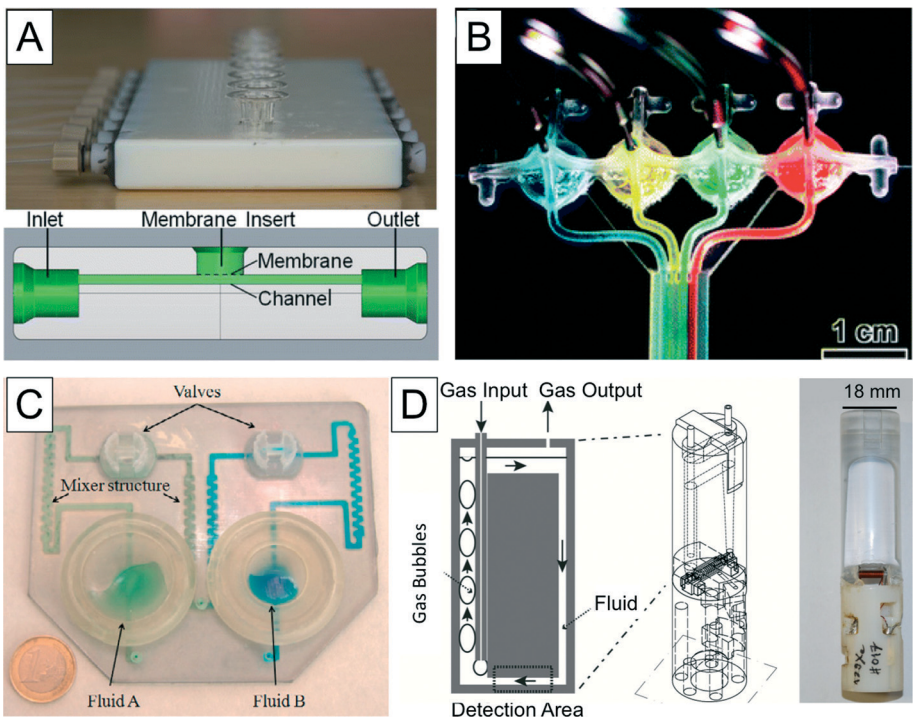

Fig. 4 Microfluidic devices printed with MJM. (A) A microfluidic device printed with Objet Connex 350 using vero white plus as the resin, incorporating adapters for syringes, 8 channels, inlets, outlets and a port for inserting a polycarbonate membrane for cell culture. (Below) side view schematic of the device. (B) A multi-flow controller device using four fluidic transistor modules, 3D-printed with a Projet 3000 HD printer, using Visijet M3 crystal photo-plastic resin. (C) A fluid mixer and homogenizer printed with Objet Eden 250 using the Full Cure 720 resin. (D) A schematic and photo of a polyjet-printed nuclear magnetic resonance (nmr) "bubble pump". Panel (A) is reproduced from ref. 46 with permission of the American Chemical Society. Panel (B) is reproduced from ref. 48 with permission of the Royal Society of Chemistry. Panel (C) is reproduced from ref. 49 with permission from elsevier. Panel (D) is reproduced from ref. 51 with permission of the Royal Society of Chemistry.

(Fig. 4C) and a microfluidic channel (375 μm square) integrated with an electrode in the wall-jet configuration was printed with an Objet Eden printer (using Full Cure 720 resin) and employed for electrochemical detection of catechol.[50] A bubble pump with vertical channels that can be closed by a separately fabricated lid has been assembled[51] (Fig. 4D). The multi-material printing property of Polyjet printing has been cleverly employed to build a lid that can be used to pressurize or pull vacuum from inlets of a microfluidic device.[52]

2.C. By fused deposition modeling

Fused deposition modeling (FDM) or "thermoplastic extrusion" is a form of 3D printing where a heated thermoplastic material is extruded from a motor-driven nozzle head that can move in three dimensions. The material hardens by spontaneous cooling immediately after extrusion. FDM was invented by Scott Crump (patent awarded in 1992) and commercialized by Stratasys. An open source development community has flourished after the expiration of the original FDM patent, leading to a number of inexpensive printers that are sold as do-it-yourself (DIY) kits or as commercial models (for example, MakerBot[53]). FDM has been used to print a wide range of cheap and biocompatible polymers like acrylonitrile butadiene styrene (ABS), poly-lactic acid (PLA), polycarbonate, polyethylene terephthalate (PET), polyamide and polystyrene. However, since the extruded material immediately hardens, the adjacent layers are not well fused, resulting in low structural strength of FDM printed objects. Incorporating a heated enclosure increases the inter-layer fusion and structural integrity, but does not eliminate the defects.[54] Recent improvements like gamma-irradiation post-printing to promote cross-linking between layers,[55] and employing thermally reversible Diels–Alder reaction to create covalent bond formation upon cooling, have resulted in increased intra-layer strength of FDM-printed objects.[54] A related strategy of FDM, where liquid precursors like metallic solutions, hydrogels, cell-laden solutions, *etc.* are extruded through a nozzle-head, has been employed to create LEDs,[56] batteries,[57] strain gauges on flexible substrates,[58] antennas,[59] interconnects,[60] and electrodes within biological tissue.[61]

Microchannel fabrication with FDM has been a challenge because of several reasons: (i) the filaments laid down by the extrusion process cannot be arbitrarily joined at channel intersections; (ii) the lack of structural integrity between the layers result in weak seals; and (iii) the size of the filaments extruded are larger than typical channels used in microfluidics. In a recent report, a fluidic channel device with a 3 mm diameter tube and 5 mm walls has been fabricated with FDM using ABS polymer; but the device leaked and could not hold over 20 bar of pressure.[62] Leroy Cronin's group showed the flow of dye solutions through FDM printed 800 μm wide channels made of polypropylene[63] (Fig. 5A), and

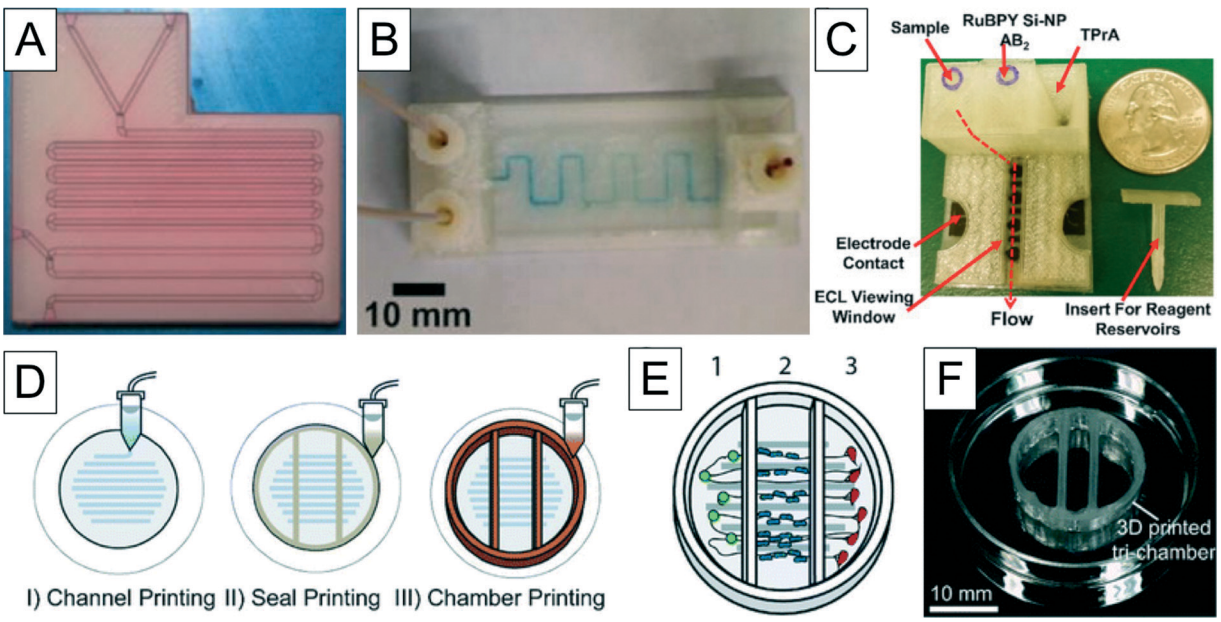

Fig. 5 Microfluidic devices printed with FDM. (A) Microfluidic device used as a chemical micro-reactor, printed in poly-propylene by FDM with a 3dtouch printer. (B) Microfluidic mixer for nanoparticle synthesis, printed with makerbot replicator 2×, by extruding pet and abs filaments for the device and the connectors respectively. (C) A microfluidic flow-based immuno-array for detecting protein biomarkers of cancer, printed with PLA, using makerbot replicator 2×. (D) Schematic drawing showing sequential printing of 350 μm wide microchannels in polycaprolactone, a silicone sealant, and a polycaprolactone cell compartmentalization chamber to make a 3D-printed nervous-system-on-a-chip device. (E) Schematic of the tri-chamber with peripheral nervous system neurons in chamber 1, Schwann cells in chamber 2, and epithelial cells in chamber 3. (F) Photograph of the nervous system on a chip device, 3D-printed with a custom printing system. Panel (A) is reproduced from ref. 63 with permission of the Royal Society of Chemistry. Panel (B) is reproduced from ref. 65 with the permission of the American Chemical Society. Panel (C) is reproduced from ref. 66 with permission from Elsevier. Panels (D)–(F) are reproduced from ref. 67 with permission of the Royal Society of Chemistry.

also built "reactionware" to hold fluids by extruding acetoxy-silicone polymer.[64] Rusling's group built microfluidic devices with 800 μm square channels (printed by extruding PET and PLA filaments) for amperometric detection of hydrogen peroxide[65] (Fig. 5B) and immuno-array based detection of cancer protein biomarkers[66] (Fig. 5C). McAlpine's group recently used a custom FDM printer to fabricate a multi-scale, biomimetic, compartmentalized nervous-system-on-a-chip device that enabled a co-culture of neurons, glia and epithelial cells.[67] The device was built by printing, first, 350 μm wide polycaprolactone microchannels (for guiding axons), followed by silicone sealant (for fluidic isolation of the chambers), and finally a tri-chamber made with polycaprolactone (for keeping the fluidic environments of the neurons, glia and epithelial cells separate) (Fig. 5D). A schematic of the device is shown in Fig. 5E and a finished device on a glass-bottom petri dish shown in Fig. 5F.

FDM also allows for creating 3D microfluidic molds in a sacrificial material that gets dissolved after the bulk material is infiltrated, thus allowing for assembly-free 3D replica-molding. Jennifer Lewis' group has fabricated complex microfluidic mixers by permeating an FDM-printed sacrificial scaffold of organic ink with a UV-curable epoxy resin and then thermally extracting the ink by heating to 60 °C (ref. 68) (Fig. 6A and B). Using a similar approach, Miller *et al.* created an endothelial cell lined vascular network embedded in an engineered tissue.[69] A sacrificial carbohydrate scaffold was FDM-printed and surrounded with live cell-laden extracellular matrix; the sugar scaffold was then dissolved with cell culture media and the voids were seeded with endothelial cells (Fig. 6C). Atala and co-workers used FDM to print human-scale engineered tissue constructs with patterns of poly-caprolactone and cell-laden hydrogel and a sacrificial polymer Pluronic F-127, which was later dissolved to form 500 μm × 300 μm microchannels for facilitating nutrient diffusion to the cells.[70] Bhargava's group employed the same approach to make a microfluidic channel network in agarose by extruding isomalt, a sugar alcohol with a glass transition temperature of 55 °C, as the sacrificial scaffold, which dissolved when surrounded by the agarose hydrogel[71] (Fig. 6D). Similarly, a 3D microchannel network in PDMS was built by curing PDMS around a FDM-printed ABS channel network, which was later dissolved in acetone.[72] The limitation of this approach is that only channels with circular cross-sections and orthogonal junctions can be fabricated, which hinders microscopy observations and might prevent such devices from being used in several key microfluidic applications such as cell separation and cell reactors.

Recently, Dolomite Microfluidics announced a desktop FDM printer, called Fluidic Factory, which is the first commercial printer specifically designed and optimized for creating completely sealed 3D microfluidic devices.[73] For creating the devices, the printer uses cyclic olefin copolymer (COC), a solvent-resistant, hard, transparent and medical-grade plastic. Although the resolution limit of the COC layers deposited by the nozzle is 320 μm (w) × 125 μm (h), the microchannel dimensions would likely be higher, because of the challenges associated with removing sacrificial layers that define the channel voids. While the printer is significantly more expensive than a MakerBot and can only produce translucent prints, the ability to create leak-free, closed and impermeable microchannels in COC with a desktop FDM printer represents an exciting development.

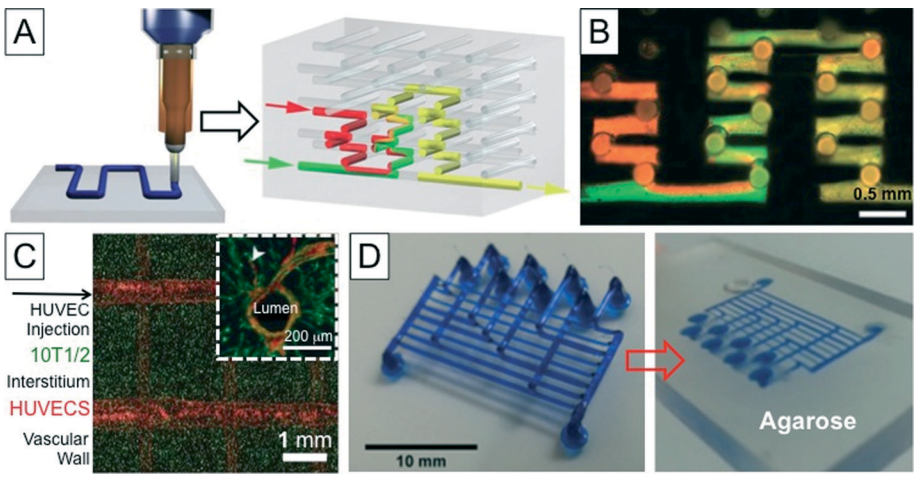

Fig. 6 Microfluidic networks produced by molding from FDM-created scaffolds. (A) Schematic of polymer extrusion, which is then removed to create a 3D microfluidic mixer. (B) Optical micrograph of a complex 3D chaotic microfluidic mixer in operation. (C) Casting of patterned vascular networks using an FDM-printed carbohydrate lattice network. The lattice structure is first surrounded with fibroblasts encapsulated in a fibrin-gel. Endothelial cells are injected into the voids created by dissolving the lattice. (Insert) endothelial (huvec) lined lumen formation surrounded by fibroblasts (10t1/2) after 9 days of culture. (D) FDM-printed sacrificial isomalt scaffold, which is then embedded in agarose for casting; the carbohydrate quickly dissolves in the agarose hydrogel and forms microchannels. Panels (A) and (B) are reprinted from ref. 68 by permission from Macmillan Publishers Ltd: nature materials, copyright 2003. Panel (C) is reprinted from ref. 69 by permission from Macmillan Publishers Ltd: nature materials, copyright 2012. Panel (D) is reproduced from ref. 71 with permission of the Royal Society of Chemistry.

3. Transition from soft lithography to 3D-printing

The microfluidics community has been understandably slow in adopting 3D-printing. Despite the advantages offered by 3D-printing over soft lithography, at present PDMS has still superior properties and there are several critical barriers that need to be overcome. As these barriers are overcome, we believe that the transition from soft lithography will be inevitable.

3.A. Advantages and disadvantages of PDMS molding

PDMS features eight key properties that have made it become the material of choice for rapid prototyping in microfluidics. PDMS is 1) easy to mold; 2) elastomeric; 3) biocompatible; 4) transparent; 5) gas-permeable; 6) impermeable to water; 7) inexpensive; and 8) copyright-free. Importantly, PDMS molding features very high resolutions; Quake has demonstrated PDMS microvalves with footprints as small as 6 μm × 6 μm.[74] However, PDMS molding suffers from the amount of manual labor involved in the fabrication process. The general procedure for molding a device in PDMS starts with the master mold (usually fabricated *via* photolithography or CNC milling), a molding process, inlet punching, and a chemical bonding step to seal the channels. However, the molding and assembly steps require extensive human labor and are difficult to automate because the exact procedure varies from design to design – so the process is not ideal for commercialization or for large-scale clinical trials. Fluidigm is an excellent example of a microfluidic-automation company that has succeeded in bringing state-of-the-art PDMS chips containing microvalve arrays to the market, but the chips cost several hundred dollars per unit. In addition, 3D PDMS designs are produced by layering and thus cannot be arbitrarily complex (*e.g.* nozzles or coils are difficult to produce). Aligning of PDMS layers in academic laboratories is challenging[75] and therefore the assembly of multi-layer PDMS devices to achieve advanced fluid routing suffers from dependence on individual skill and poor reproducibility.[76] High-throughput molding of plastics by injection molding is available but the cost of the metallic molds can be an obstacle for prototyping and commercialization and is also limited by layered design.[1]

3.B. Critical barriers that have prevented the adoption of 3D-printing

Despite the above-mentioned limitations of soft lithography, the microfluidics community has been slow in adopting 3D-printing because this new technology still has its limitations. The features and barriers that distinguish 3D-printing from soft lithography and are most relevant for the microfluidics community are summarized in Table 1. Interestingly, the strengths and limitations of 3D-printing have historically been almost the mirror image of those of PDMS molding: 3D-printing is a fully digital, automated 3D technique (minimal labor, no assembly), however microfluidic engineers are legitimately concerned about the cytocompatibility of the resins used for building the microchannels and also the insufficient patterning resolution or throughput for manufacturing microfluidics (PDMS molding also suffers from low throughputs).

On the other hand, the current resolution of commercial 3D-printers does not match yet what is routinely achievable by soft lithography and we are still on the lookout for a versatile and biocompatible resin that matches PDMS. Both 3D-printing techniques and soft lithography suffer from low throughput. However, the fast pace of innovation in SL- and MJM-based 3D-printing in the last 2 years, primed by the expiration of key patents and the emergence of competing platforms, is ushering in significant improvements in resolution and throughput.

3.C. Overcoming the critical barriers

3.C.1. Resolution improvements in 3D-printing. Present 3D-printing techniques have not yet matched the kind of resolutions that are required, for example, to stretch single DNA molecules,[83] and are achievable with PDMS or plastic-based micromolding. Multi-photon SL systems are capable of micron-level resolutions, but their high costs severely hinder their dissemination beyond academic research. Below we review the major resolution limitations in 3D-printing systems.

Most of the commercially-available desktop SL-printers are ill-equipped to pattern transparent resins because they feature visible-spectrum light sources (405 nm laser or visible-light DLP). Since SL resins typically have a significantly higher absorbance at lower wavelengths, UV light sources can increase the Z-resolution of SL-printing.[82] Some manufacturers have started selling 385 nm UV-LED DLP-based desktop SL printers (Phoenix Touch Pro by Full Spectrum Laser 3D[84] and Pico2 and Pro2 from Asiga[85]) with higher resolutions. However the build size in these commercial printers is reduced in order to improve resolution. For microfluidic applications, while high resolution is important, so is the build area, which should at least be compatible with standard glass slides that are 75 mm long.

Simulations and finite element modeling (FEM) has been used to model the complex process of photo-polymerization and estimate the exposure parameters for achieving the highest possible z-resolution. Partial differential equations describing (1) the DMD pixel or laser source light intensity profile,[86,87] (2) the penetration of UV into the liquid monomer solution (Beer–Lambert law),[14,88] (3) the chemical kinetics related to polymer chain initiation, propagation and termination,[89] (4) the thermodynamics of chemical bond formation during polymerization,[14] and (5) the diffusion of the photo-initiator and radicals through the partially polymerized resin[14,88] need to be solved to get a good *a priori* estimate of the expected resolution. The depth of curing assumes particular importance when building the roof of microchannels, since light penetration into the void of the channels can partially cure the resin, making it hard to

Table 1 Comparison between various features of PDMS-based soft-lithography and three 3D printing techniques that are most relevant to microfluidics (SL, MJM and FDM)

		3D-printing		
Features	Soft lithography	Stereolithography	Multi-jet modeling	Fused deposition modeling
1 3D-capability	Partially achieved by stacking and bonding multiple layers – connections between channels in different layers can only be orthogonal	Very little topological restriction in 3D architecture. Only dimensional limits. High optical absorption is required to create microchannel roof	Very little topological restriction in 3D architecture. Only dimensional limits. A sacrificial layer is required to build the microchannel roof	Limited to circular channel cross-sections and orthogonal junctions
2 Resolution (of microchannels)	Very high (inherited from photolithography). Limited by diffraction.	Current: ~100 μm channels[77] with opaquing agent	Current: ~300 μm voids[48] (750 μm channels)	Current: ~350 μm (ref. 67)
	5 μm wide channels are standard. Sub-micron resolution possible with appropriate photomasks	Hydrodynamic limit: draining channels of viscous, uncured resin	Removal of support material is diffusion-limited (slow for long narrow channels)	
3 Material properties				
a. Chemical composition	PDMS (open-source)	Proprietary photoresins (Somos, Ormocer, Fototec, FormLabs, BV, Watershed, *etc.*)	Proprietary photocurable polymers (Visijet, FullCure, Vero)	Open-source thermoplastics (ABS, PLA, polycarbonate, polyphenylsulfone, polypropylene, polyamide, COC, *etc.*)
		PEG-DA (open-source)		
b. Solvent compatibility	Water-impermeable	Commercial resins are water-resistant. Varying resistance to organic solvents (Somos 5530HT, 9920 is resistant to most solvents, Watershed is not resistant to ethanol). Higher MW hydrogel resins are not water or solvent resistant	Data not available (for resins available from Stratasys, 3D Systems)	Thermoplastics are water resistant. Varying chemical resistance[78]
	Swells in organic solvents			
c. Gas permeability	Well-studied high gas permeability[79]	Most SL resins are hard plastics with poor gas permeability; commercial elastomeric SL resins are typically sold uncharacterized	Data not available (for resins available from Stratasys, 3D Systems)	Most FDM thermoplastics are hard plastics with poor gas permeability
d. Surface derivatization and wettability	Wettable when surface is oxidized (plasma).[80] Oxidized PDMS can be derivatized with silanes	Wettability can be modulated with resins terminated with special groups, or by silane modification and silicate coatings	Data not available (for resins available from Stratasys, 3D Systems)	Plasma oxidation can turn most of the FDM plastics hydrophilic
e. Mechanical strength	Elastomer – Young's modulus (360–870 kPa)[81]	Young's modulus vary with material – Ormocer (1–4 GPa), WaterShed (2.7 GPa)	Young's modulus vary with material – FullCure720 (1.5–2 GPa), Visijet M3 (1–2 GPa)	Young's modulus (ABS, PC, PPS, COC: ~2–3 GPa)
	Isotropic strength	Minimal anisotropy in mechanical properties[54]	Build orientation can affect elastic modulus[54]	Anisotropy in strength – inter-layer bonding weak[54]
f. Optical clarity	Clear and transparent	Clear resins: Watershed, Visijet SL Clear, BV-003, Form-Clear, PEG-DA (MW 258)[82]	Clear resins: MED610, RGD720	Clear resins: ABS, COC
	Depends on surface roughness of the mold	Depends on surface roughness of vat & build plate (SL), volume defects and light-absorbing additives		
4 Biocompatibility	Biocompatible and bio-functional	Many resins are cytotoxic and not biocompatible. WaterShed and Visijet SL Clear are USP Class VI plastic. PEG-DA is biocompatible	MED610 is a USP VI, biocompatible plastics	Many biocompatible thermoplastics available – ABS, PLA, PC, COC, PP, *etc.*
5 Multi-material fabrication	Possible with bonding	Possible with some advanced SL printers	Easily possible	Possible

Table 1 *(continued)*

		3D-printing		
Features	Soft lithography	Stereolithography	Multi-jet modeling	Fused deposition modeling
6 Digital Inspection	Inaccuracies in assembly of 3D devices make FEM simulations of the complete device only approximate	FEM simulation of the complete device can predict the performance of the device prior to fabrication/printing. The constraints of each fabrication technique apply		
7 Automated Manufacturing	Not possible	Semi-automated. Post-processing needed to drain channels of uncured precursor[31] and to remove support structures	Semi-automated. Post-processing needed to remove sacrificial material from the channel	Fully automated
8 Throughput	Low	Low, but higher than PDMS molding.[31] As the design grows in complexity, the throughput difference between 3D-Printing and PDMS grows larger		

remove after printing. Using photo-absorbing additives like Sudan Black with PEG-DA,[90] Nordin and colleagues have systematically studied the minimal (non-transparent) channel dimensions that can be reliably printed with SL (60 μm (h) × 108 μm (w))[77] (Fig. 7).

The ability to clear the uncured (or partially-cured) resin (in SL) or sacrificial polymers (in MJM) from the finished channels after completion of the printing process is an additional and important factor in determining the resolution of 3D-printed microchannels. In fact, for long channels, this "hydrodynamic" limitation can be more significant than the constraints imposed by light scattering and diffusion of the polymer precursors. Strategies to facilitate resin removal post-printing, like short-cut holes, or temporary breakable connectors, can be incorporated at the design stage. Newer less viscous resins will also make drainage easier, thereby making higher resolution channels possible. Since some post-processing and resin removal needs to be done manually after printing, SL-based and MJM-based manufacturing of microfluidic devices can be termed as a *quasi-automated*, *quasi-additive* fabrication process (FDM can be fully automated). This additional step of resin clearance adds to the cost of manufacturing and could become significant in high-volume applications.

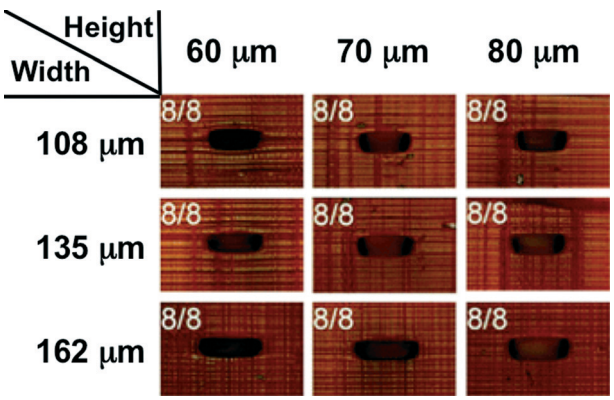

Fig. 7 Channel resolution in 3D printing. The smallest microchannels that have been consistently printed have been fabricated with PEG-DA by addition of 0.6% of the opaquing agent Sudan 1. The figure is adapted from ref. 77 with permission of the Royal Society of Chemistry.

With the expiration of all the major SL patents in 2014, the market has seen the advent of many manufacturers pushing the boundaries on resolution. Desktop machines with ~20 μm horizontal resolution and 6 μm vertical resolution[91] and with multi-material capability[91,92] are now commercially available. Many DLP-based SL printers now have open and modular architecture; in the near future, modular DLP-based SL printers will improve as the DLPs are upgraded.

3.C.2. Throughput improvements in 3D-printing systems. Recent technical innovations, particularly the "continuous printing" SL approaches described earlier, have increased the printing speeds by over two orders of magnitude,[18,93–95] which has brought down the printing time from hours to minutes (for a 51 mm diameter complex spherical test object[93]). While injection molding can produce a device per second and is still indispensable for large-scale production, SL printers are now very well placed in terms of cost and throughput for low and medium-volume batch productions. This throughput capability should prove ideal for rapid prototyping, classroom projects, personalized medicine, and clinical trials.

3.C.3. Materials research. One of the primary reasons for the success of soft lithography for microfluidic device fabrication has been the optimal material properties of PDMS – PDMS is transparent, biocompatible, flexible, gas-permeable, relatively inexpensive, and moldable with high fidelity and simplicity. 3D-printing resins, in contrast, have historically

been expensive, pigmented or colored, and toxic or largely incompatible with live biological material. Not surprisingly, the unsuitability of the printing material has been a big deterrent for biomedical scientists to adopt 3D-printing. However, in the last few years, considerable attention is being paid to create new 3D-printing materials with more desirable properties.

3.C.3.1. Biocompatibility. For 3D-printed devices to become applicable in biomedical research and clinical settings, resins must have experimentally confirmed biocompatibility. A thorough investigation on the biosafety and biofunctionality of the available resins is required. Hardly any comprehensive biosafety study has been conducted with most commercially available resins, many of which have proprietary formulations.

While most proprietary resins for use with commercial 3D-printers have not been assessed for their biosafety and biofunctionality, cell encapsulation in photo-crosslinked hydrogels is a well-researched area that has demonstrated the biocompatibility of some potential candidate resins for SL. Biocompatible hydrogel matrices made with poly-ethylene-glycol-diacrylate (PEG-DA),[96–99] poly-ethylene-glycol-dimethacrylate,[100] gelatin methacrylate,[101,102] hyaluronic acid[103] and functionalized methacrylic alginates[104] modified with cell-attachment proteins or peptide moieties, have been used to stereolithographically encapsulate neurons or myocytes[104] (Fig. 8A), fibroblasts[96,105] (Fig. 8B) and human mesenchymal stem cells.[106] Shear and co-workers have used multi-photon lithography to excite photo-sensitizers like Rose Bengal and methylene blue and fabricate micro-chambers with protein-crosslinked walls around gelatin-embedded bacterial communities[107] (Fig. 8C). Bio-actuators and biosensors incorporating live myocytes have been 3D-printed with collagen hydrogels[108,109] (Fig. 8D–G), and could in principle be used for long-term studies of muscle cell differentiation.[110,111]

A few resins have already undergone some biocompatibility certifications. A SL-resin, Somos Watershed 11122 XC (DSM, Netherlands), and MJM-resins, VisiJet M3 Crystal (3D Systems, USA) and MED610 (Objet/Stratasys, USA) have been certified as USP Class VI or "medical-grade" plastic. MED610 and Watershed has met more stringent biocompatibility standards – ISO 10993-5 (cytotoxicity) and ISO 10993-10 (irritation and delayed-type hypersensitivity) – whereas MED610 has also passed ISO-10993-3 (genotoxicity), ISO-10993-18 (chemical characterization of organic and aqueous extracts) and ISO-13485 (every batch of material undergoes biocompatibility testing) certifications. However, FDA approves devices, not

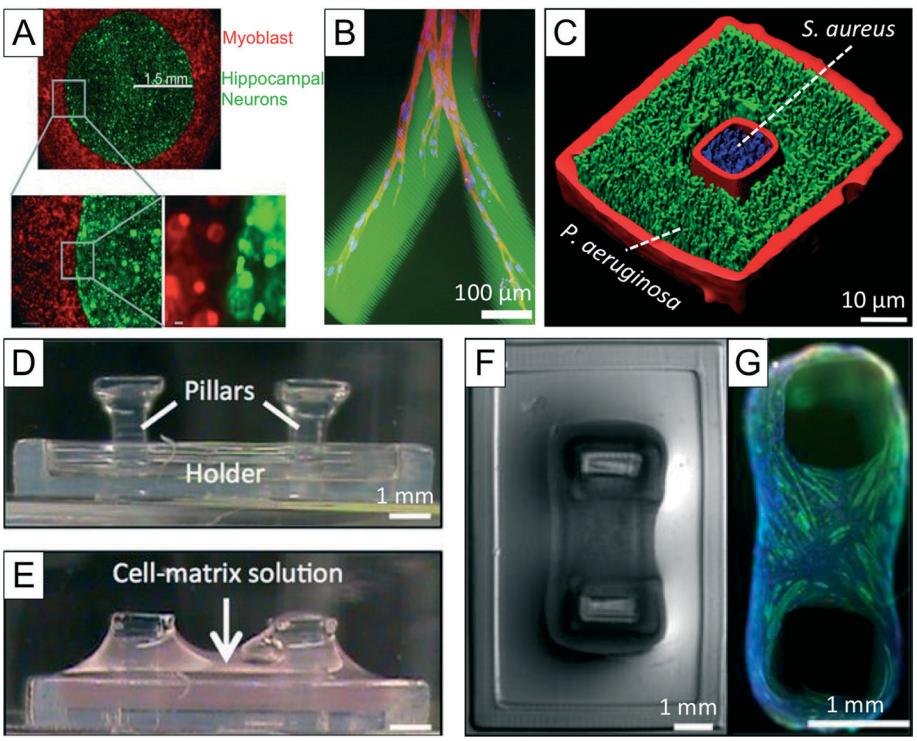

Fig. 8 Biocompatibility of resins used in bio-printing. (A) Mouse hippocampal neurons (green) and skeletal muscle myoblast cells (red) encapsulated in OMA-PEGMA1100 hydrogels, are spatially patterned in distinct regions, with multi-material SL-printing. (B) Confocal image showing human dermal fibroblast cells (red) undergoing 3D migration within a RGDS-functionalized region (green) of a SL-printed PEG hydrogel. (C) Microclusters of the bacteria *S. aureus* (blue) printed within high-density populations of *P. aeruginosa* (green) in bsa-gelatin micro-containers (red). (D) SL-printed PEG-DA "biobot" structure. (E) C2C12 myoblast cells mixed with matrigel and matrix proteins deposited on the "bio-bot" structure. (F) Cells formed a compact and solid muscle strip around the PEG-DA structure. (G) Immunostaining of the cells with mf-20 (green) and dapi (blue). Panel (A) is reproduced from ref. 104 with permission from Wiley-VCH. Panel (B) is reproduced from ref. 105 with permission from Elsevier. Panel (C) is reproduced from ref. 107 with permission from the National Academy of Sciences. Panels (D)–(G) have been reproduced from ref. 108 with permission of the National Academy of Sciences.

materials – so these certifications do not automatically make the plastics safe to use in all biomedical applications; more specific and longer-term studies need to be performed on the printed devices for ascertaining their biosafety and biofunctionality.

Analyzing the leachates from printed objects is critical for biosafety assessment. A couple of recent studies presented a comprehensive toxicity profiling of the leachates of some commercially available resins and polymers that are commonly used in 3D printing – ABS (FDM), PLA (FDM), VisiJet Crystal (MJM), Visijet SL Clear (MJM), Watershed 11122 XC (SL), Dreve Fototec 7150 Clear (SL), Form 1 Clear (SL).[112,113] Zhu *et al.* observed significant growth inhibition in freshwater microalgae when they were cultured for 48–96 hours in water-soluble leachate extracted from all 3D-printed structures.[112] Aqueous extracts from all SL polymers induced 100% mortality of *Daphnia sp.* neonates after 24 hours, and all SL and MJM polymers proved to be significantly toxic to zebrafish embryos[112] (Fig. 9D). Zebrafish embryos cultured in 3D-printed structures made of Visijet Crystal or Watershed showed developmental defects,[112,113] whereas those grown in leachate extracts of ABS and PLA did not have any behavioral abnormalities.[112]

UV-irradiation to cure unreacted monomers and post-printing extensive washes often prove to be sufficient for rendering the printed objects safe for cell culture and biomedical applications. With SL, we have printed PEG-DA (MW = 258) petri dishes, which were rendered cytocompatible after overnight UV curing and 24 hour extraction of leachates in water. The PEG-DA (MW = 258) petri dishes were compatible for the long-term (>3 days) growth of mammalian cell lines (CHO-K1) (Fig. 9E), which were indistinguishable from cells grown on tissue culture polystyrene (TCPS) surfaces (Fig. 9F). Additionally, the PEG-DA surfaces functionalized with Matrigel also supported the growth of more delicate primary embryonic hippocampal neurons (Fig. 9G). Note that PEG-DA (MW = 258) has very low levels of autofluorescence, allowing for fluorescence microscopy observations (Fig. 9E).[82]

Many of the polymers used in FDM printing (such as ABS and PLA) are very biocompatible.[114] Cell-laden bio-inks made with purified ECM proteins[70] or from de-cellularized tissue-derived ECM[115] have been FDM-printed along with synthetic biodegradable polymers like polycaprolactone (PCL). A few FDM-printed microfluidic devices have also been used with cell cultures. Recently, Johnson and co-workers FDM-printed a compartmentalized device with polycaprolactone to create a

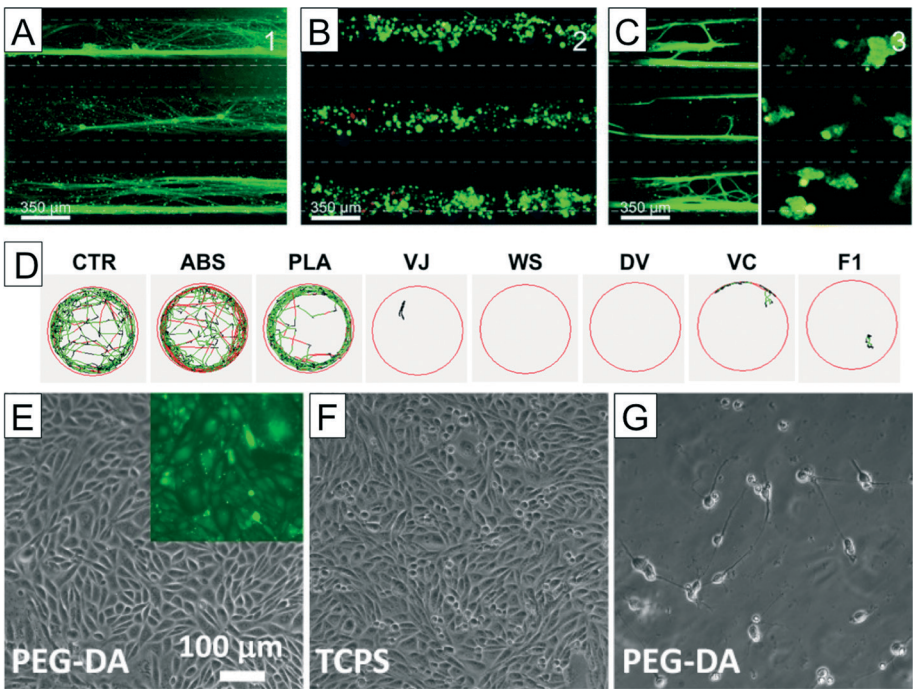

Fig. 9 Biocompatibility of 3D-printed devices. (A) Fluorescence micrographs showing three parallel FDM-printed polycaprolactone microchannels, with axons (stained for tau) from superior cervical ganglion neurons growing in chamber 1 of the device shown in Fig. 5E. (B) Fluorescence micrographs of three parallel poly-caprolactone microchannels with axon-associated Schwann cells in chamber 2 of the device in Fig. 5e. (C) Fluorescence micrograph of axon-terminals and epithelial cells (cytokeratin stained in green) in chamber 3 of the device in Fig. 5e. (D) Toxicity profiling of different 3D-printed polymer extracts using the vertebrate zebrafish model – larvae trajectories after 5 minutes of exposure with the polymer extracts. ABS—acrylonitrile butadiene styrene; PLA—poly(lactic) acid; VJ—Visijet Crystal; WS—Watershed 11122xc; DV—Dreve Fototec 7150 Clear; VC—Visijet SL Clear; F1—Form 1 Clear. (E) Chinese hamster ovary (CHO-K1) cells growing on SL-printed PEG-DA-258 surfaces. (Inset) fluorescence image of CHO-K1 cells stained with cell tracker green. (F) CHO-K1 cells cultured on tissue-culture polystyrene surface for comparison with (E). (G) Hippocampal neurons from embryonic day 18 mouse cultured on 3D-printed PEG-DA surfaces coated with poly-D-lysine and matrigel at div 3. Panels (A)–(C) are reproduced from ref. 67 with permission of the Royal Society of Chemistry. Panel (D) is reproduced from ref. 112 with permission of the American Institute of Physics.

multi-scale model of the peripheral nervous system (see section 2.C, Fig. 5E). Peripheral nervous system neurons from the superior cervical ganglion extended axons through the microchannels (Fig. 9A). Schwann cells (glia) cultured in the second chamber wrapped around the axons (Fig. 9B) and epithelial cells growing in the third chamber interacted with the axon terminal (Fig. 9C). The fluidic isolation between the three chambers enabled the establishment of distinct environments for each cell-type.

Advances made in the drug-delivery field also throw light on the biocompatibility of some of the resins that have been used to fabricate microneedles with SL (Fig. 3B). Microneedles made by Matsuda and Mizutani, with a custom acrylate resin containing polycaprolactone, elicited an inflammatory reaction when implanted, which could be suppressed by loading the needles with the anti-inflammatory drug, indomethacin.[116] Commercially-available acrylate-based polymers (e-Shell 200 and 300), that are Class IIa biocompatible, have been used to fabricate microneedles and hearing aids.[22,117] Ormocer, a material that has been used to create high-resolution features (50 μm wide channels)[118] and sharp microneedle tips by SL,[119–121] has supported the growth of human epidermal keratinocytes for 3 days without significant loss in viability.[120]

Many research efforts have been directed towards improving the photoinitiators, which are the source of much of the cytotoxic effects. Elisseeff and colleagues systematically analyzed the biosafety of photo-initiators used for cell encapsulation in photo-polymerized hydrogels by including post-processing steps like repeated washes and UV-curing, and found that Irgacure-2959 had relatively low cytotoxicity.[122] Liska and co-workers also characterized different photo-polymer combinations for SL and showed that Irgacure-819 and Diinone also had relatively low toxicity in cells.[123,124] Anseth and colleagues developed a superior UV-sensitive and visible-light photo-initiator lithium phenyl-2,4,6-trimethylbenzoylphosphinate (LAP) that required lower concentrations and reduced light intensities for photo-curing, and consequently showed greater viability of encapsulated cells.[125]

Although some of the initial biosafety and biocompatibility studies of 3D-printed devices are encouraging, longer-term *in vitro* cytotoxicity studies and *in vivo* implant compatibility still needs to be ascertained. In addition, more research needs to be conducted to fully characterize the bio-fouling properties of the resins. We believe that, as soon as resin research moves to optimize materials for biomedical applications, we should see the development of a new variety of resins that are not only biocompatible but also non-fouling, implantable and/or bio-resorbable.

3.C.3.2. Transparency. The optical clarity or the transparency of a printed device depends on 2 factors: (a) the absorptivity of the material in the visible spectrum; and (b) the roughness on the surface and defects within the bulk that can cause diffraction of light. Since the inter-layer fusion is weak in FDM printed devices, they suffer the most in terms of optical clarity (*e.g.* COC is a very transparent polymer, but FDM-printed microfluidic devices made with Dolomite's Fluidic Factory are translucent). There are several SL resins that are marketed as "clear" (*e.g.* Watershed, Form Labs Clear, Visijet SL Clear, BV-003), but depending on the surface finish resulting from clearing of the channel interior walls, they are translucent at best; the SEM of a 250 μm microchannel made with the Miicraft SL printer shows the surface roughness of the interior walls.[25] The build orientation in SL can determine whether the roof or the sidewalls of a channel are rough and plays a critical role in the transparency of the final printed device.[31] Urrios *et al.* have improved the transparency in SL by printing against a smooth vat surface and a smooth build plate[82] (Fig. 10A). It is important to note that some resins, such as Watershed, become yellow after prolonged exposure (months) to ambient light (Fig. 10B).

3.C.3.3. Multi-material printing. Multi-material printing is an inherent capability of MJM and FDM. Ismagilov's group has reported a clever microfluidic pump based on two-material MJM; the seal of the pump was printed with an elastomeric material whereas the rest of the pump was printed with a hard plastic (see section 3.D.5).[52] SL, on the other hand, has been traditionally limited to single materials. Recent advances in SL printers and resins have pushed the boundaries into printing with multiple resins[126] (Fig. 11A), including elastomers[127] (Fig. 11B) and ceramics,[128] as well as resins encapsulating different cell-types[96] (Fig. 11C–D). When

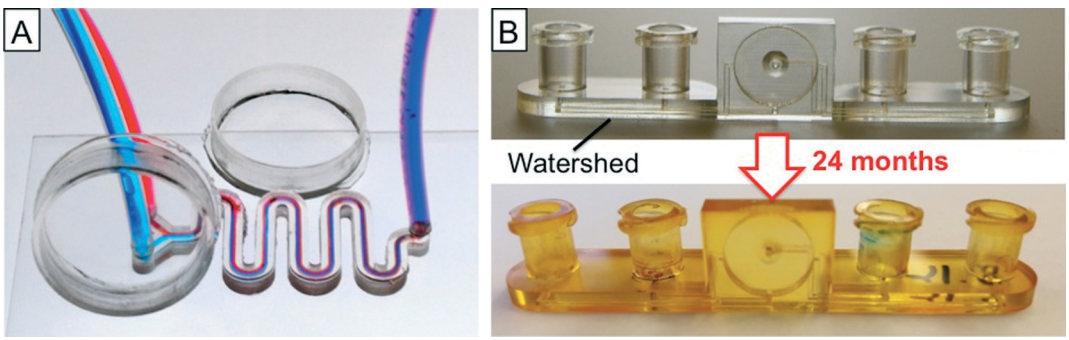

Fig. 10 Transparency of 3D-printed devices. (A) A transparent microfluidic channel and petri-dishes SL-printed with PEG-DA (MW 258). (B) Watershed is a very transparent SL-resin but turns yellow after prolonged exposure to ambient light.

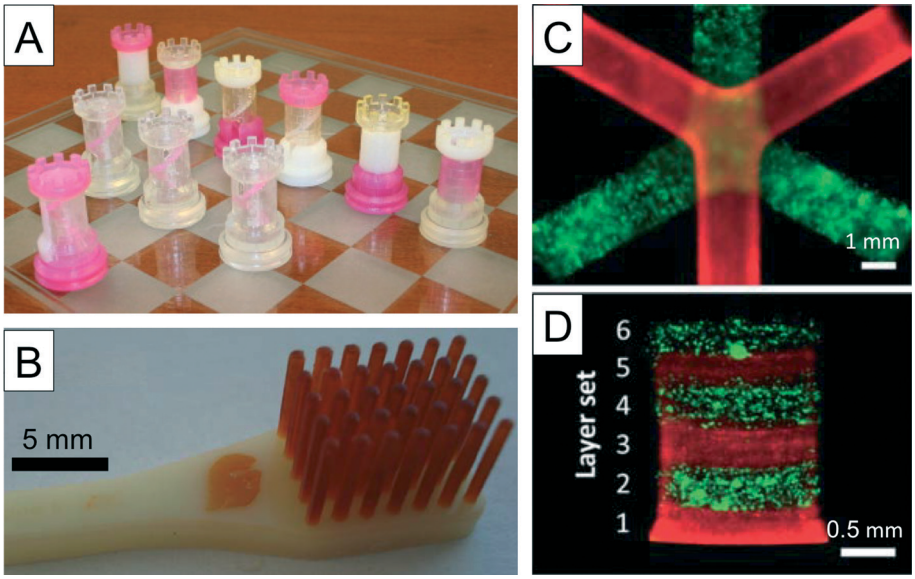

Fig. 11 Multi-material SL printing. (A) Various rooks fabricated with 4 different commercially available photo-resins, using a custom-built multi-material SL-printer. (B) A 2-material SL print – the red bristles are made of an elastomeric resin. (C) NIH-3t3 fibroblasts stained with different colored cell tracker dyes and encapsulated in PEG-DA hydrogels, SL-printed in different layers. (D) Cross-sectional view of the SL printed (~500 μm) layers of encapsulated NIH-3t3 cells. Panel (A) is reproduced from ref. 126 with permission of the authors. Panel (B) is reproduced from ref. 127 with permission of the authors. Panel (C) and (D) are reproduced from ref. 96 with permission of the Royal Society of Chemistry.

copper microparticles were added to a photoresin, a sintering process made the printed structures conductive (~10 times less than pure copper).[129] In the not too distant future, integrated 3D-printed devices with metallic sensors and actuators on flexible membranes,[130] or polymer gradients with novel properties, will become a reality with a new generation of multi-material SL printers.[91]

3.C.3.4. Wettability. The wettability of the channel walls is a property that assumes particular significance in 3D-printed materials, in order to facilitate easy passage of aqueous fluids through the microchannels. PDMS, although extremely hydrophobic, can be easily treated with oxygen plasma to create a hydrophilic surface. In addition, PDMS is highly gas-permeable, so trapped bubbles can easily be dislodged by pressurizing the fluid in the channel.[79] SL-printed plastics and MJM resins do not have the same degree of gas permeability and therefore the bubble-removal trick that works so well in PDMS channels, does not work as well with SL- and MJM-printed channels. Efforts are now on to create hydrophilic resins that enable spontaneous filling of microchannels with aqueous solvents – for example, by using vinyl-terminated initiators in the resin base, to produce polymers like poly(ethylene glycol) methacrylate (PEGMA) and perfluorodecyl methacrylate (PFMA) with enhanced hydrophilicity.[131] FDM thermoplastics, on the other hand, are either hydrophilic or easily rendered hydrophilic *via* an oxygen plasma treatment after printing.

3.C.3.5. Surface derivatization and bonding. Derivatization of the surface of channels post-fabrication is important for a variety of reasons, *e.g.* preferentially altering the hydrophilicity or making the surface chemically reactive/inert. Silanes have been extensively used for modifying the PDMS surface to change its wettability, to make it amenable for bonding, or for covalently attaching chemical species.[132] Lately, silane chemistry has been exploited to modify the surface of SL resins. One strategy has been to coat the walls of a channel with a silicate coating by injecting a hydrolyzed ethyl silicate solution (N-103X, Colcoat Co.) and heating it to allow the solution to vaporize and coat the inside walls of the channel.[133] Silicates have been used traditionally as the base surface on which silane chemistry has been performed. The Hayakawa group derivatized the silicate surface with a fluorosilane, thereby making it possible for the device to generate monodisperse inverted water-in-oil emulsions.[134] Silane modification, followed by a phase conversion of allylhydridopolycarbosilane, can generate hydrophilic silicate-glass coatings inside the microchannels, which can confer excellent solvent resistance, and drive high electro-kinetic flow, while retaining transparency.[135] Alternatively, siloxane layers have been deposited on epoxy-based SL-resins by treating the surface with 3-glycidoxypropyltrimethoxysilane (GPTMS) under acidic pH in the presence of a photo-acid generator, triarylsulfonium hexafluoroantimonate (TASHFA),[136] or with dimethoxydimethylsilane (DMDMS) using a heat induced sol–gel process.[137] Siloxane groups form the backbone of silicones, including PDMS; therefore, siloxane derivatized SL-resins can be bonded to PDMS surfaces to make hybrid devices.

3.C.3.6. Solvent compatibility. PDMS is a very porous, hydrophobic matrix. As a result, PDMS swells up in various organic solvents. This swelling leads to the loss of solvent, or other hydrophobic constituents in the fluid, into the PDMS matrix. Undesired exposure of PDMS to organic solvents often produces deformed channel geometries and detachment of the seal between the channel walls and the

surface. The incompatibility of PDMS with organic solvents has led to multiple research efforts into making microfluidic devices with more chemically resistant materials like Viton[138] or Teflon.[139]

There is a diversity of resins with a range of compatibility to solvents and resistance to chemicals. Somos 9920 is an SL resin that has great chemical resistance and is suitable, like polypropylene, for long-term storage of a variety of chemicals. Watershed (Somos 11120), on the other hand, a medical grade and transparent resin, is very resistant to water but not to organic solvents, including ethanol.

3.D. The promise of 3D printing

3.D.1. Towards true 3D capability. Microfluidic devices made from molding PDMS or plastics have to be built by stacking and bonding different layers together – a process which increases the final cost of the devices and drastically limits the connectivity of the various parts of a device and the overall functionality of the devices. 3D-printing, on the other hand, is an assembly-free technology, limited only by the resolution constraints of the printing process. There are very few topological restrictions (*e.g.* "floating" objects cannot be printed and have to be tethered), which opens the doors to 3D design innovation. For example, an efficient 3D micromixer architecture,[20] diaphragms with sinusoidal cross-sections,[48] a spiral channel with trapezoid cross-sections,[24] and integrated connectors[31] are a few examples of microfluidic devices where the functional elements were enabled by 3D design. Moreover, microfluidic engineers can now take advantage of very large CAD repositories of 3D digital objects available online for free. A notable example is GrabCAD,[140] a fully searchable library that contains more than one million CAD designs and also offers a free design platform for engineering teams to streamline projects.

3.D.2. Towards rational design. Modular designs and integrated interfaces come naturally to the rational "CAD approach" in 3D-printing. With 3D-printing, industry-standards for fluid interfacing, like Luer Lock and barb fittings, can be seamlessly integrated and built into the microdevice.[31] Inspired by the Lego® bricks concept, functional and modular elements of a complex microfluidic circuit, have been printed by SL, and assembled by a "plug-and-play" interlocking mechanism, into a complete microfluidic device[141–145] (Fig. 12). A

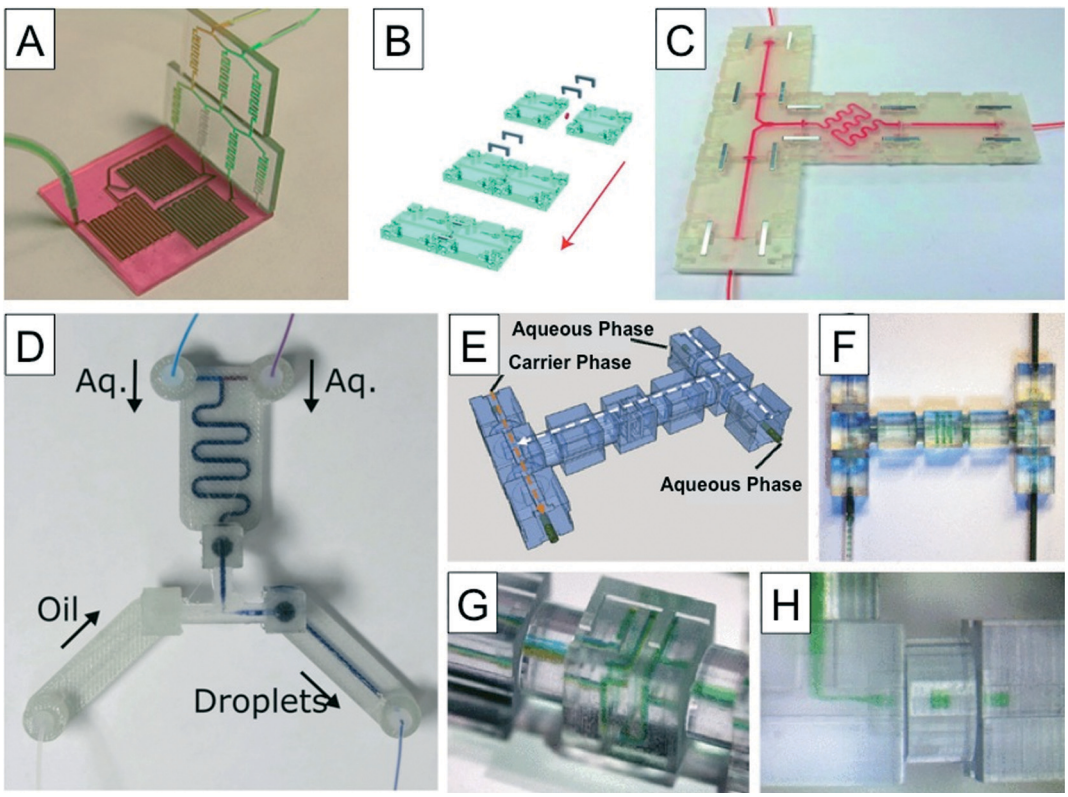

Fig. 12 Modular microfluidics. (A) A modular microfluidic mixer built by SL. (B) Schematic assembly of different 3D-printed microfluidic blocks with metal pins to build an entire device. (C) An integrated microfluidic device for biosensing built by connecting different functional modules printed in Visijet M3 crystal with Projet HD 3500 plus. (D) An interconnected modular device for generating oil-in-water droplets, 3D-printed with PLA using ultimaker FDM-printer. (E) A cad drawing of a t-junction droplet generator, built by mating discrete microfluidic elements, SL-printed with watershed. (F) Operation of the t-junction emulsification device. (G) Two dye-colored aqueous streams mixed in a 3D helical mixer, and (H) formed into droplets after getting sheared by a carrier oil phase. Panel (A) is reproduced from ref. 142 with the permission of the Royal Society of Chemistry. Panel (B) and (C) are reproduced from ref. 144 with the permission of the Royal Society of Chemistry. Panel (D) is reproduced from ref. 145 under the Creative Commons Attribution License. Panel (E)–(H) are reproduced from ref. 143 with the permission of the National Academy of Sciences.

tunable microfluidic mixer and a droplet generator are examples of complex microfluidic devices that have been demonstrated by assembling SL-printed discrete functional modules[143,146] (Fig. 12E–H).

The concept of "modular design" can be extended beyond interlocking *physical modules* to coupling different *digital modules*, and fabricating them as a monolith. With the digital modular approach, 3D-printing can bring in a paradigm shift in microdevice design by catalyzing collaborations between the designers that have different expertise in the various modules that form a device. We foresee a future when a non-specialist user can virtually assemble a microdevice for his/her niche experimental purpose by digitally putting together various microfluidic functional modules that are accessible online. The user can then model the performance of the device using available finite-element software, and finally fabricate them using SL-printing service facilities. At present, a single engineer designs most of the PDMS-based microfluidic platforms in a non-standardized and non-modular way. In contrast, large teams of engineers in, say, the electronics and automobile industry, often in different geographical locations, design various functional units, which are then assembled digitally into the final product. We believe that the adoption of SL as a microfluidic design tool will enable modular design and integration of devices, a strategy that has become the norm in various successful industries.

Historically, soft lithography has been a notoriously inefficient fabrication process, in contrast with 3D-printing. Complex microfluidic devices made by aligning and assembling different PDMS layers often have dimensions that are significantly different from the desired "ideal CAD" version and cannot be accurately determined *a priori*. Therefore, any prediction of the final performance of a complex multi-layer PDMS device based on the "ideal CAD" version is often found to be quite different from the real performance. Almost always, many iterations of the design are necessary due to design mistakes and the fabrication process needs to be repeated before an optimally operating device is sent to manufacturing. On the other hand, one of the biggest advantages of 3D printing is that the digital 3D design enables the user to predict the final performance of a device using finite element modeling before the device is printed. Such digital inspection allows for efficient remote collaboration and a more rational approach to design. We believe that by drastically reducing the number of fabrication iterations in the development of a complex device, this rational "CAD approach" will save significant time and resources.

3.D.3. Towards user-friendly interfaces. The absence of standardization in interfacing PDMS microdevices with the peripherals ("chip-to-world" connection) has been a major bottleneck in the widespread adoption of lab-on-a-chip technologies. The inlet/outlet connectors and tubing often remain one of the most unreliable components in a device. Moreover, the profusion of tubings and interconnects that have to be individually connected for a microdevice with multiple fluid inputs and control lines,[147] can soon become very intimidating for the end-user. The recent push for translatable and commercially viable products by funding agencies and society is starting to generate more attention towards user-friendliness of microdevices. We believe that 3D-printing is uniquely positioned not only to facilitate standardization of interfaces, but also to promote user-friendly design in microfluidics[30,31,148] (Fig. 13).

3.D.4. Towards 3D-printed automation. Many biomedical applications require repetitive fluid handling – transferring fluid from one container to another and mixing fluids constitute the most common actions. Traditionally, such fluid handling has been done using manually-operated pipettes, a

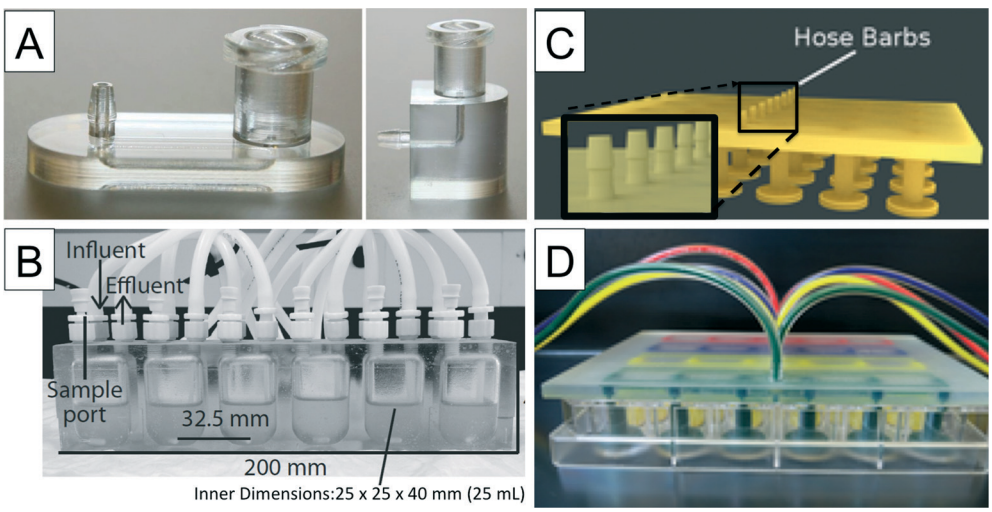

Fig. 13 3D-printed user-friendly interfaces. (A) Luer and barb connectors integrated with a microfluidic channel SL-printed with watershed. (B) A complex bioreactor with integrated inlet and outlet ports printed with SL. (C) Schematic of an integrated SL-printed oxygen control insert for a 24 well plate – the inlet and outlet barbs allow perfusion of oxygen into the wells. (D) Photo of an entire 24-well plate fitted with the oxygen control insert that it filled with dyes for visualization. Panel (B) is reproduced from ref. 148 with the permission of American Society of Microbiology. Panel (C) and (D) are reproduced from ref. 30 under the Creative Commons CC0 License.

process that is error-prone, time-consuming, costly and extremely tedious. In industrial laboratories, expensive robotic dispensers have largely replaced humans. Microfluidic technology has introduced the ability to handle and manipulate extremely small volumes of fluids in miniaturized lab-on-a-chip formats that has enabled massive parallelization, reduced reagent costs and accelerated reaction times or processing. However, in order to achieve complete automated fluidic handling in lab-on-a-chip devices, valves and pumps are indispensable.[147] The invention of PDMS microvalves and micropumps by the Quake group revolutionized the field of microfluidics and heralded the miniaturization and automation of many kinds of biomedical assays.[149,150] Yet the manufacturability of the microvalves due to the cumbersome alignment, bonding and assembly of small flexible parts has remained a challenging hurdle.[151]

The Folch lab SL-printed diaphragm valves and peristaltic pumps designed for microfluidic automation.[152] The valve is operated pneumatically by pressurizing a control line that deflects a 10 mm-diam., 100 μm-thick Watershed membrane and closes a nozzle at ~6 psi (Fig. 14A). The valves are completely leakage-free at the closing pressure, and can be operated over many closing cycles, at frequencies up to ~7 Hz. The 3D-printed valves can be regarded as functional modules – two valves can be paired to build a switch, three valves can be put together in series to build a peristaltic pump, *etc.* (Fig. 14B). A four-way switch was used to control ATP perfusions of CHO-K1 cells and read their real-time calcium-imaging fluorescent responses in a 3D-printed Watershed cell culture chamber (Fig. 14C). Nordin and colleagues have SL-printed 80–100 μm 2 mm-diam. Membrane valves with PEG-DA that close 250 μm tall × 350 μm wide channels at ~20 psi.[153] These PEG-DA valves were actuated at 1 Hz and remained functional for ~800 cycles. However since the resin formulation used for making the valves has Sudan 1 as an absorber, the devices are not optically transparent. Sochol *et al.* recently published the design of an integrated diaphragm with a sinusoidal cross-section as a dynamic microfluidic element.[48] The diaphragm was 3D-printed by MJM, and was used in various configurations as a fluidic capacitor, diode, and transistor (Fig. 14D–G).

We envision that valves and pumps 3D-printed at low cost with transparent biocompatible plastics will enter the market to automate fluid handling and manipulation in the biotech and biomedical industry, replacing costly human labor and even robotic dispensers. However, to design a truly large-scale integrated microfluidic circuit, further miniaturization of the dynamic microfluidic elements is crucial. Improvements in the 3D printing process such as better resolution and higher-biocompatibility resins will be required.

3.D.5. Towards autonomous systems. The accessibility of microfluidic devices is limited by the need to tether these devices to bulky and expensive peripherals, like pumps, gas canisters, and controllers.[154] The absence of topological

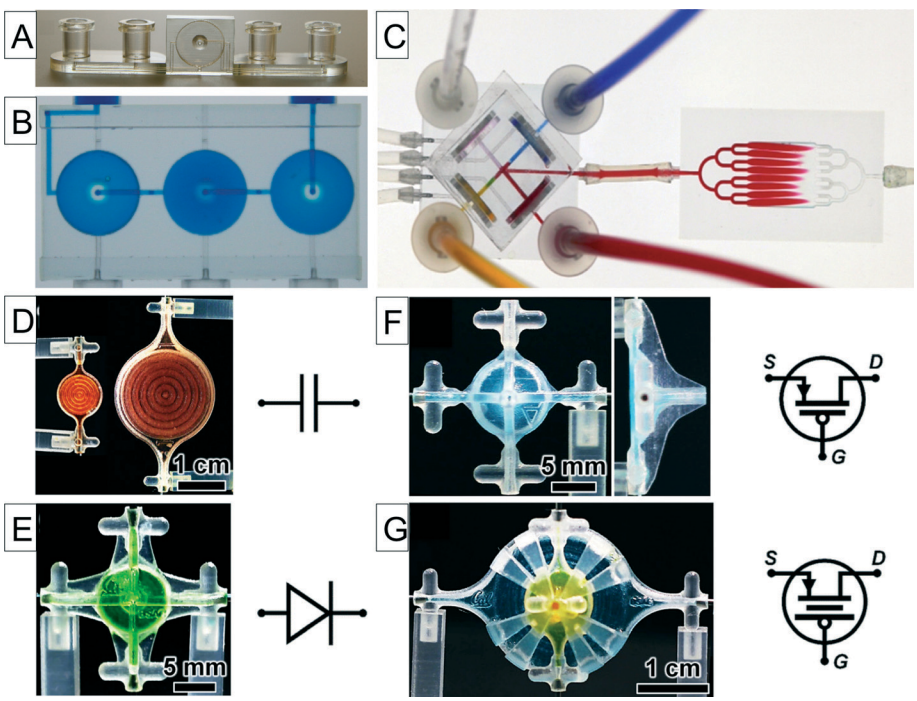

Fig. 14 3D-printed automation. (A) Photograph of a SL-printed single-valve device made with watershed resin. (B) A peristaltic pump designed with three valves in sequence, during an actuation phase when only the middle valve is open. (C) Photograph of an actuating switch connected to a cell-culture chamber. Only the valve connected to the red dye solution is open. (D)–(G) Dye-filled fluidic circuit control elements printed with Visijet M3 crystal using a Projet 3000 HD printer and their respective analogous electrical symbols – (D) fluidic capacitors, (E) fluidic diode, (F) fluidic transistor and (G) enhanced-gain fluidic transistor. Panels (A)–(C) are reproduced from ref. 152 with the permission of the Royal Society of Chemistry. Panels (D)–(G) are reproduced from ref. 48 with the permission of the Royal Society of Chemistry.

constraints in 3D printing has led to some innovative solutions in untethered fluid automation. The Ismagilov lab has used multi-material MJM to construct an "equipment-free pumping lid" for controlled pressure generation in microfluidic devices[52] (Fig. 15). When the lid is pushed into a cup that is integrated to the inlets of a microfluidic device, the air in the lid's cavity is compressed and generates positive pressure. Similarly, when the lid is pulled up from a pre-placed position in the cup's cavity, a negative pressure is created. A guiding structure determines the distance the lid travels inside the cup's cavity and therefore controls the generated pressures. By eliminating external pressure sources and controllers, the pumping lid technology can be used for driving microfluidic flow for over 2 hours, which is sufficient for many applications.

Digital electronics took a quantum leap when logic gate circuits could be put together to design complex logic elements, and autonomous systems. We predict that 3D-printed valves will also simplify the fabrication and consequently popularize logic elements in microfluidics, such as memory latches,[155] shift-registers,[156] adding-machines,[157] oscillators[158,159] and autonomous pumps.[160] We can envision 3D-printed, truly autonomous microfluidic machines with embedded controls (powered by flow or a manually-generated pressure differential) that can run pre-programmed biochemical and cell-based assays without the use of pneumatics, electricity, or tubing.

3.D.6. Towards web-based dissemination of designs and devices. 3D-printing is a new technology that is benefiting from an old concept: the scalability of digital systems. Pioneers in Internet and computer science predicted very early, how computers would change the world. Professor Robert Licklider from MIT, one of the main architects of the early ARPANet, wrote a seminal paper, "*Man-Computer Symbiosis*" (1960),[161] where he introduced the revolutionary idea that computers could help humans make decisions just as humans were helping computers. Elaborating on this idea, his protégé Douglas Engelbart at Stanford further argued in 1962 ("*Augmenting Human Intellect*: *A Conceptual Framework*")[162] that computer networks develop an "amplified intelligence" as the number of users of the network grows.

Engelbart's idea has engendered a thriving 3D-printing industry. Several popular web based 3D-printing services (*e.g.*, www.shapeways.com, www.sculpteo.com, i.materialise.com, *etc.*), focusing primarily on the jewelry, art and home decor sectors, are allowing designers to publish their designs in a "virtual marketplace". The user-designer can now start "monetizing" (obtaining revenue from) their design through convenient ecommerce platforms as soon as other users 3D-print copies of their design from the virtual marketplace. Thanks to these 3D-printing services, designers do not have to face the administrative, logistical and financial challenges of setting up a physical shop or worry about distribution costs – considerations that are crucial for designers at the beginning of an enterprise. Two key features of this new manufacturing process that fundamentally distinguishes it from the classical "thick-paper-catalog" model of R&D marketing are: 1) the designer is not required to order expensive molds and set up a company for launching production of his/her devices; and 2) the customer does not have a "minimum quantity" limit and

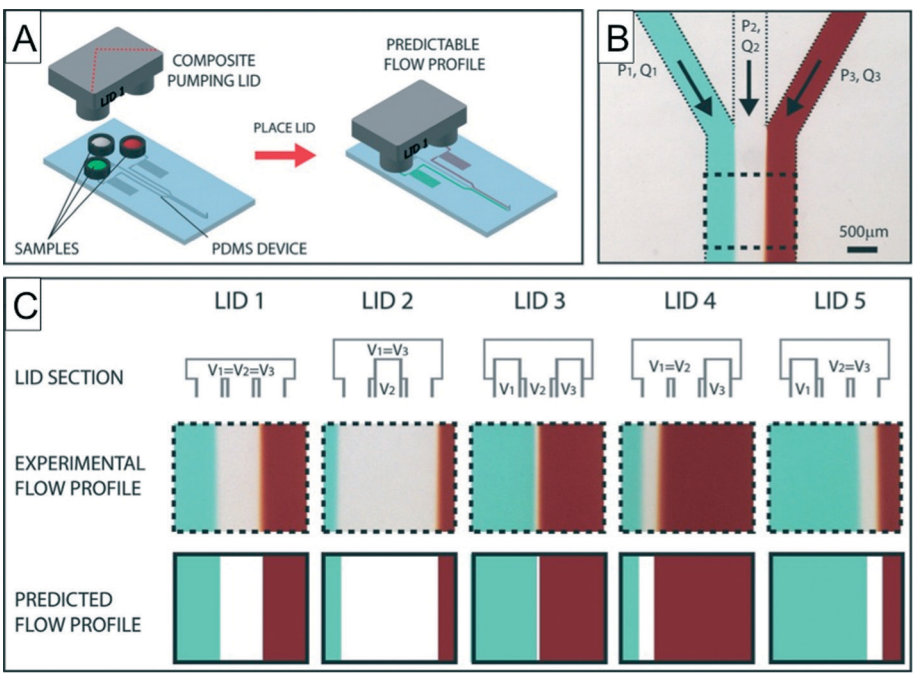

Fig. 15 The "pumping lid". (A) Schematic of a three-cup composite pumping lid for producing three different pressures in the same device. (B) Micrograph of the junction at which three channels combine to produce a heterogeneous laminar flow. (C) Different composite lids (top row schematics) can be used to produce different flow profiles (middle row) that agree very well with the predictions of the flow profiles (bottom row) based on the pressures produced by the lids and the device geometry. Reproduced from ref. 52 with permission of the Royal Society of Chemistry.

can order even a single print. MakerBot has also created a very dynamic website (called "Thingiverse"[53]) for sharing CAD designs with only non-commercial (Creative Commons[163]) licenses. Over time, we believe that these 3D-printing marketplaces will generate dynamic communities of "amplified intelligence" creating designs that we cannot even imagine today. As Tim Berners-Lee, the inventor of the World Wide Web, put it, "what you create is limited only by your imagination".[164]

Important note on safety

3D-printers are often hailed as a very safe technology. As a result, they are usually sold with a front plastic panel as the only protecting interface and operated without proper protection garment. 3D-printing technology does not entail the dangers of silicon etching or laser micromachining, but we have found that long-term exposure presents some hazards:

1) Any 3D-printer that generates fumes or odors should be placed under a laminar flow extractor or inside a fume hood. All SL printers and all FDM systems fall under this category. Polyjet printers also produce "smelly" prints and should be in a well-vented room. In general, vapors from molten polymers and low-vapor-pressure molecules such as photoinitiators and monomers can be irritants to the respiratory system and, as such, should be considered potential carcinogens. Odors from laboratory compounds have resulted in damage to the olfactory epithelium and irreversible loss of olfaction.[165]

2) SL resins are particularly dangerous compounds because they become activated with light. If unexposed resin becomes in contact with a user's skin, and the skin is exposed to light, the user can face severe rashes and/or burns upon generation of free radicals by the resin's photoinitiator. This exposure can happen inadvertently through gloves or through garment, particularly with transparent (colorless) resins.

3) Safety goggles should be worn for SL until the end of processing to avoid exposure of the eyes to SL resins. Resins are severe irritants to the eye tissue. Goggles should also be worn during post-processing (when flushing the channels), as small amounts of resin could splash into the eye when attempting to flush the channel.

4. Conclusions

To better understand the suitability of the different manufacturing strategies for microfluidics, we compare soft lithography, injection molding, paper microfluidics and 3D-printing on several pertinent factors like set-up cost, cost/print, turn around time, 3D design capability, fluidic automation, throughput and manufacturability (Table 2). Injection molding is justified for large production runs if (and only if) a large-enough capital investment can be safely secured; in this case, very low costs per device can be achieved. Paper microfluidics is an attractive approach for devices with simple functionality, because of its low setup and running costs and high throughput. On the other hand, both injection molding and paper microfluidics are not well suited for automated fluid manipulation. Soft lithography is the only technique that has been routinely used to fabricate valves and pumps for fluidic automation. However, high set up and running costs and low throughput limit the manufacturability of PDMS-based devices.

Unlike all other strategies, 3D printing is the only technique with true 3D digital design capability. Moreover, microfluidic devices with integrated valves and pumps have recently been demonstrated with two different 3D-printing techniques. Additive manufacturing techniques are efficient because they (a) favor modular and team-based CAD, (b) does not require tooling or assembly, (c) generate very little waste, and (d) lower distribution costs. When all costs (capital, time, personnel, disposal, *etc.*) are factored in, the economics usually favor 3D-printing for low- to mid-scale production, even when it is based on serial fabrication.

A quick bibliometric analysis of the microfluidics field shows that, in the last 5 years, after a steady growth that lasted a decade, the number of publications has reached a plateau (at around 6500 publications per year in 2013, as measured in Web of Science) and even slightly decreased (Fig. 16A, inset). Poor manufacturability of PDMS devices may be discouraging researchers to adopt PDMS technology for the dissemination of their inventions (*i.e.* the manufacturability roadblock alluded to in section 1), and might be a reason for the plateauing of publications. It has been argued that microfluidics produces very few "killer applications",[166,167] or products that reach the consumer market. Here we argue that there is no dearth of "killer app" ideas – it is the commercialization pipeline that is hindered by critical barriers. We hypothesize that, once 3D-printing becomes a mature technology and overcomes its own critical barriers, we will undoubtedly see a microfluidic revolution in biomedicine and biotechnology.

Table 2 Comparison of microfluidic device manufacturing strategies

	Soft lithography	Injection molding	Paper microfluidics	3D printing
Setup cost	~$80k[a]	>$50k[b]	<$1k	$1–20k
Cost per print/materials	High	Low	Low	High
Turn-around time	~24 h	3 weeks[c]	<2 h	<2 h
3D capability	Layered 2D designs	Layered 2D designs	Layered 2D designs	3D digital designs
Fluid automation	Routine	Difficult	Rudimentary	Demonstrated
Throughput	Low	Very high	High	Medium
Manufacturability	Poor	Poor	Good	Good

[a] Based on quotes from Black Hole Laboratories. [b] Based on quotes for basic injection molding apparatus. [c] Based on estimates from Proto Labs.

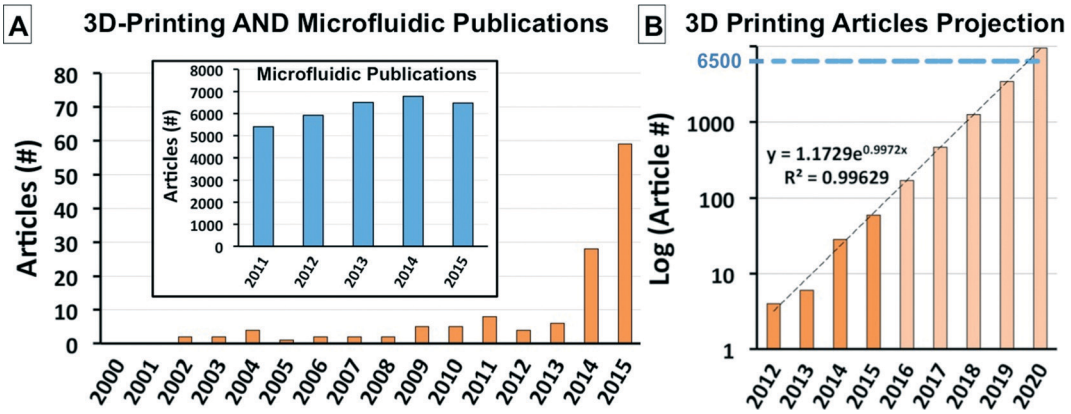

Fig. 16 Publication trends. (A) Bar-graph showing the total number of publications per year (in web of science) with keywords "3D-printing" (including "additive manufacturing", "three-dimensional printed", *etc.*) and "microfluidic" from 2000–2015. (Inset) bar-graph showing the total number of publications per year (in web of science) in microfluidics in the last 5 years (2011–2015). (B) Projection of the exponential growth in the number of publications in 3D-printed microfluidics, based on the recent trend (from 2012–2015).

In support of our hypothesis, one of the few areas in microfluidics that is experiencing a rapid growth is 3D-printed microfluidic devices (Fig. 16A). While 3D-printing does not provide high-throughput (like injection molding of thermoplastics or paper microfluidics do), it is the only fabrication strategy that possesses three key characteristics essential to researchers: low-cost setups, rapid prototyping and 3D digital design, which results in good manufacturability. (Paper microfluidics also feature good manufacturability but are inadequate for key biotechnological processes such as fluid automation and live cell culture.) Not surprisingly, the number of publications on 3D-printed microfluidics is experiencing an exponential growth. At this rate, the number of publications on 3D-printed microfluidics will total half the present number of publications in mid-2018 and outnumber it by March 2020 (Fig. 16B).

In this review we have seen that this rapid growth is marked by low-cost developments, by an emphasis on materials research (biocompatible resins) and hardware improvement (multi-material printing, high-throughput printing, *etc.*), and by exploiting 3D design capabilities. We believe that, in the short term, this growth will have its largest biomedical impact in the same areas where PDMS microfluidics did through the advent of microfluidic automation: in molecular biology, genomics, cell biology – where the need to manipulate small amounts of fluid volumes in large quantities and repetitively becomes inhumanely tedious and economically prohibitive. For simple reasons of cost, we will soon see 3D-printing take a leading technological role in global health care (mostly prototyping diagnostic devices for the third world) as well as a substitute of precision-machining for R&D instrumentation and in the acceleration of clinical trials. In the long term, the largest impact might be in the very lucrative clinical sector of personalized devices (not necessarily microfluidic), such as implants and prosthetics.

In conclusion, the revolutionary aspect of 3D-printing is that it minimizes the barriers to manufacturing. Enabling rapid prototyping of a physical model in a few hours is already revolutionizing the product design process by allowing microfluidic engineers to test designs before investing in photomask tooling or mold fabrication processes. In biomedicine, expediting the translation from prototype to product should enable personalized devices and therapy, accelerate R&D, and help make healthcare more affordable and accessible.

Acknowledgements

A. U. is a recipient of a "La Caixa" fellowship from Catalonia and a European Molecular Biology Organization (EMBO) short-term fellowship. We acknowledge partial support from the National Institutes of Health (1R01NS064387) for N. B.

References

1 H. Becker and L. E. Locascio, *Talanta*, 2002, **56**, 267–287.
2 E. K. Sackmann, A. L. Fulton and D. J. Beebe, *Nature*, 2014, **507**, 181–189.
3 S. R. Shankar and D. G. Jansson, in *Concurrent Engineering: Contemporary Issues and Modern Design Tools*, ed. H. R. Parsaei and W. G. Sullivan, Springer US, 1993.
4 E. Roy, J.-C. Galas and T. Veres, *Lab Chip*, 2011, **11**, 3193–3196.
5 M. Focke, D. Kosse, C. Müller, H. Reinecke, R. Zengerle and F. von Stetten, *Lab Chip*, 2010, **10**, 1365–1386.
6 N. S. Cameron, H. Roberge, T. Veres, S. C. Jakeway and H. J. Crabtree, *Lab Chip*, 2006, **6**, 936–941.
7 A. Manz, N. Graber and H. M. Widmer, *Sens. Actuators, B*, 1990, **1**, 244–248.
8 A. W. Martinez, S. T. Phillips and G. M. Whitesides, *Proc. Natl. Acad. Sci. U. S. A.*, 2008, **105**, 19606–19611.
9 A. Mazzoli, *Med. Biol. Eng. Comput.*, 2013, **51**, 245–256.
10 D. A. Zopf, S. J. Hollister, M. E. Nelson, R. G. Ohye and G. E. Green, *N. Engl. J. Med.*, 2013, **368**, 2043–2045.
11 B. Duan and M. Wang, *MRS Bull.*, 2011, **36**, 998–1005.
12 P. J. Bártolo, *Stereolithography: Materials, Processes and Applications*, Springer US, 2011.

13 A. Waldbaur, H. Rapp, K. Länge and B. E. Rapp, *Anal. Methods*, 2011, **3**, 2681–2716.
14 N. Fang, C. Sun and X. Zhang, *Appl. Phys. A: Mater. Sci. Process.*, 2004, **79**, 1839–1842.
15 A. Bertsch, S. Zissi, J. Y. Jezequel, S. Corbel and J. C. Andre, *Microsyst. Technol.*, 1997, **3**, 42–47.
16 A. Bertsch, P. Bernhard, C. Vogt and P. Renaud, *Rapid Prototyp. J.*, 2000, **6**, 259–266.
17 B. C. Gross, J. L. Erkal, S. Y. Lockwood, C. Chen and D. M. Spence, *Anal. Chem.*, 2014, **86**, 3240–3253.
18 J. R. Tumbleston, D. Shirvanyants, N. Ermoshkin, R. Janusziewicz, A. R. Johnson, D. Kelly, K. Chen, R. Pinschmidt, J. P. Rolland, A. Ermoshkin, E. T. Samulski and J. M. DeSimone, *Science*, 2015, **347**, 1349–1352.
19 H.-W. Kang, I. H. Lee and D.-W. Cho, *J. Manuf. Sci. Eng.*, 2004, **126**, 766–771.
20 A. Bertsch, S. Heimgartner, P. Cousseau and P. Renaud, *Lab Chip*, 2001, **1**, 56–60.
21 C.-H. Hsu and A. Folch, *Appl. Phys. Lett.*, 2006, **89**, 144102.
22 P. R. Miller, S. D. Gittard, T. L. Edwards, D. M. Lopez, X. Xiao, D. R. Wheeler, N. A. Monteiro-Riviere, S. M. Brozik, R. Polsky and R. J. Narayan, *Biomicrofluidics*, 2011, **5**, 13415.
23 W. Lee, D. Kwon, B. Chung, G. Y. Jung, A. Au, A. Folch and S. Jeon, *Anal. Chem.*, 2014, **86**, 6683–6688.
24 W. Lee, D. Kwon, W. Choi, G. Y. Jung, A. K. Au, A. Folch and S. Jeon, *Sci. Rep.*, 2015, **5**, 7717.
25 A. I. Shallan, P. Smejkal, M. Corban, R. M. Guijt and M. C. Breadmore, *Anal. Chem.*, 2014, **86**, 3124–3130.
26 T. Femmer, A. Jans, R. Eswein, N. Anwar, M. Moeller, M. Wessling and A. J. C. Kuehne, *ACS Appl. Mater. Interfaces*, 2015, **7**, 12635–12638.
27 J. M. Zhang, E. Q. Li, A. A. Aguirre-Pablo and S. T. Thoroddsen, *RSC Adv.*, 2016, **6**, 2793–2799.
28 T. Kanai and M. Tsuchiya, *Chem. Eng. J.*, 2016, **290**, 400–404.
29 W. G. Patrick, A. A. K. Nielsen, S. J. Keating, T. J. Levy, C.-W. Wang, J. J. Rivera, O. Mondragón-Palomino, P. A. Carr, C. A. Voigt, N. Oxman and D. S. Kong, *PLoS One*, 2015, **10**, e0143636.
30 M. D. Brennan, M. L. Rexius-Hall and D. T. Eddington, *PLoS One*, 2015, **10**, e0137631.
31 A. K. Au, W. Lee and A. Folch, *Lab Chip*, 2014, **14**, 1294–1301.
32 A. Selimis, V. Mironov and M. Farsari, *Microelectron. Eng.*, 2015, **132**, 83–89.
33 C. N. LaFratta, J. T. Fourkas, T. Baldacchini and R. A. Farrer, *Angew. Chem., Int. Ed.*, 2007, **46**, 6238–6258.
34 B. Kaehr and J. B. Shear, *J. Am. Chem. Soc.*, 2007, **129**, 1904–1905.
35 M. Malinauskas, M. Farsari, A. Piskarskas and S. Juodkazis, *Phys. Rep.*, 2013, **533**, 1–31.
36 B. Kaehr and J. B. Shear, *Proc. Natl. Acad. Sci. U. S. A.*, 2008, **105**, 8850–8854.
37 R. Nielson, B. Kaehr and J. B. Shear, *Small*, 2009, **5**, 120–125.
38 B. Kaehr and J. B. Shear, *Lab Chip*, 2009, **9**, 2632–2637.
39 B.-B. Xu, Y.-L. Zhang, H. Xia, W.-F. Dong, H. Ding and H.-B. Sun, *Lab Chip*, 2013, **13**, 1677–1690.
40 A. Pilipović, P. Raos and M. Šercer, *Int. J. Adv. Des. Manuf. Technol.*, 2009, **40**, 105–115.
41 D.-G. Ahn, J.-Y. Lee and D.-Y. Yang, *J. Mech. Sci. Technol.*, 2006, **20**, 19–28.
42 Y. L. Cheng and S. J. Chen, *Mater. Sci. Forum*, 2006, **505-507**, 1063–1068.
43 B. O. Erbano, A. C. Opolski, M. Olandoski, J. A. Foggiatto, L. F. Kubrusly, U. A. Dietz, C. Zini, M. M. M. A. Marinho, A. G. Leal and R. Ramina, *Acta Cir. Bras.*, 2013, **28**, 756–761.
44 S. G. Bucella, G. Nava, K. C. Vishunubhatla and M. Caironi, *Org. Electron.*, 2013, **14**, 2249–2256.
45 J. L. Erkal, A. Selimovic, B. C. Gross, S. Y. Lockwood, E. L. Walton, S. McNamara, R. S. Martin and D. M. Spence, *Lab Chip*, 2014, **14**, 2023–2032.
46 K. B. Anderson, S. Y. Lockwood, R. S. Martin and D. M. Spence, *Anal. Chem.*, 2013, **85**, 5622–5626.
47 S. Y. Lockwood, J. E. Meisel, F. J. Monsma and D. M. Spence, *Anal. Chem.*, 2016, **88**, 1864–1870.
48 R. D. Sochol, E. Sweet, C. C. Glick, S. Venkatesh, A. Avetisyan, K. F. Ekman, A. Raulinaitis, A. Tsai, A. Wienkers, K. Korner, K. Hanson, A. Long, B. J. Hightower, G. Slatton, D. C. Burnett, T. L. Massey, K. Iwai, L. P. Lee, K. S. J. Pister and L. Lin, *Lab Chip*, 2016, **16**, 668–678.
49 A. Bonyár, H. Sántha, B. Ring, M. Varga, J. Gábor Kovács and G. Harsányi, *Procedia Eng.*, 2010, **5**, 291–294.
50 A. S. Munshi and R. S. Martin, *Analyst*, 2015, **141**, 862–869.
51 A. Causier, G. Carret, C. Boutin, T. Berthelot and P. Berthault, *Lab Chip*, 2015, **15**, 2049–2054.
52 S. Begolo, D. V. Zhukov, D. A. Selck, L. Li and R. F. Ismagilov, *Lab Chip*, 2014, **14**, 4616–4628.
53 MakerBot, http://www.makerbot.com.
54 J. W. Stansbury and M. J. Idacavage, *Dent. Mater.*, 2016, **32**, 54–64.
55 S. Shaffer, K. Yang, J. Vargas, M. A. Di Prima and W. Voit, *Polymer*, 2014, **55**, 5969–5979.
56 Y. L. Kong, I. A. Tamargo, H. Kim, B. N. Johnson, M. K. Gupta, T.-W. Koh, H.-A. Chin, D. A. Steingart, B. P. Rand and M. C. McAlpine, *Nano Lett.*, 2014, **14**, 7017–7023.
57 K. Sun, T. S. Wei, B. Y. Ahn, J. Y. Seo, S. J. Dillon and J. A. Lewis, *Adv. Mater.*, 2013, **25**, 4539–4543.
58 J. T. Muth, D. M. Vogt, R. L. Truby and Y. Mengüç, *Adv. Funct. Mater.*, 2014, 6307–6312.
59 J. J. Adams, E. B. Duoss, T. F. Malkowski, M. J. Motala, B. Y. Ahn, R. G. Nuzzo, J. T. Bernhard and J. A. Lewis, *Adv. Mater.*, 2011, **23**, 1335–1340.
60 A. Joe Lopes, E. MacDonald and R. B. Wicker, *Rapid Prototyp. J.*, 2012, **18**, 129–143.
61 M. S. Mannoor, Z. Jiang, T. James, Y. L. Kong, K. A. Malatesta, W. O. Soboyejo, N. Verma, D. H. Gracias and M. C. McAlpine, *Nano Lett.*, 2013, **13**, 2634–2639.
62 A. J. Capel, S. Edmondson, S. D. R. Christie, R. D. Goodridge, R. J. Bibb and M. Thurstans, *Lab Chip*, 2013, **13**, 4583–4590.
63 P. J. Kitson, M. H. Rosnes, V. Sans, V. Dragone and L. Cronin, *Lab Chip*, 2012, **12**, 3267–3271.

64 M. D. Symes, P. J. Kitson, J. Yan, C. J. Richmond, G. J. T. Cooper, R. W. Bowman, T. Vilbrandt and L. Cronin, *Nat. Chem.*, 2012, **4**, 349–354.
65 G. W. Bishop, J. E. Satterwhite, S. Bhakta, K. Kadimisetty, K. M. Gillette, E. Chen and J. F. Rusling, *Anal. Chem.*, 2015, **87**, 5437–5443.
66 K. Kadimisetty, I. M. Mosa, S. Malla, J. E. Satterwhite-Warden, T. M. Kuhns, R. C. Faria, N. H. Lee and J. F. Rusling, *Biosens. Bioelectron.*, 2016, **77**, 188–193.
67 B. N. Johnson, K. Z. Lancaster, I. B. Hogue, F. Meng, Y. L. Kong, L. W. Enquist and M. C. McAlpine, *Lab Chip*, 2016, **16**, 1393–1400.
68 D. Therriault, S. R. White and J. A. Lewis, *Nat. Mater.*, 2003, **2**, 265–271.
69 J. S. Miller, K. R. Stevens, M. T. Yang, B. M. Baker, D.-H. T. Nguyen, D. M. Cohen, E. Toro, A. A. Chen, P. A. Galie, X. Yu, R. Chaturvedi, S. N. Bhatia and C. S. Chen, *Nat. Mater.*, 2012, **11**, 768–774.
70 H.-W. Kang, S. J. Lee, I. K. Ko, C. Kengla, J. J. Yoo and A. Atala, *Nat. Biotechnol.*, 2016, **34**(3), 312–319.
71 M. K. Gelber and R. Bhargava, *Lab Chip*, 2015, **15**, 1736–1741.
72 V. Saggiomo and A. H. Velders, *Adv. Sci.*, 2015, **2**, 1500125.
73 Dolomite Microfluidics, http://www.dolomite-microfluidics.com/webshop/fluidic_factory.
74 I. E. Araci and S. R. Quake, *Lab Chip*, 2012, **12**, 2803–2806.
75 A. Folch and M. A. Schmidt, *J. Microelectromech. Syst.*, 1999, **8**, 85–89.
76 J. Y. Kim, J. Y. Baek, K. A. Lee and S. H. Lee, *Sens. Actuators, A*, 2005, **119**, 593–598.
77 H. Gong, M. Beauchamp, S. Perry, A. T. Woolley and G. P. Nordin, *RSC Adv.*, 2015, **5**, 106621–106632.
78 W. Woishnis and S. Ebnesajjad, *Chemical resistance of thermoplastics*, William Andrew Publishing, 2012.
79 T. C. Merkel, V. I. Bondar and K. Nagai, *J. Polym. Sci., Part B: Polym. Phys.*, 2000, **38**, 415–434.
80 D. C. Duffy, J. C. McDonald, O. J. Schueller and G. M. Whitesides, *Anal. Chem.*, 1998, **70**, 4974–4984.
81 D. Armani, C. Liu and N. Aluru, *Micro Electro Mech. Syst.*, 1999, 222–227.
82 A. Urrios, C. Parra-Cabrera, Gonzalez-Suarez, N. Bhattacharjee, L. Rigat-Brugarolas, U. Nallapati, J. Samitier, C. DeForest, F. Posas, J. Garcia-Cordero and A. Folch, *Lab Chip*, submitted.
83 J. M. Sidorova, N. Li, D. C. Schwartz, A. Folch and R. J. Monnat, *Nat. Protoc.*, 2009, **4**, 849–861.
84 Full Spectrum Laser, http://www.fsl3d.com.
85 Asiga, http://www.asiga.com.
86 C. Sun, N. Fang, D. M. Wu and X. Zhang, *Sens. Actuators, A*, 2005, **121**, 113–120.
87 H. W. Kang, J. H. Park and D. W. Cho, *Sens. Actuators, A*, 2012, **178**, 223–229.
88 K. Bhole, P. Gandhi and T. Kundu, *J. Appl. Phys.*, 2014, **116**, 043105.
89 A. S. Jariwala, F. Ding, A. Boddapati, V. Breedveld, M. A. Grover, C. L. Henderson and D. W. Rosen, *Rapid Prototyp. J.*, 2011, **17**, 168–175.
90 M. P. Lee, G. J. T. Cooper, T. Hinkley, G. M. Gibson, M. J. Padgett and L. Cronin, *Sci. Rep.*, 2015, **5**, 9875.
91 Ilios, http://www.ilios3d.com.
92 3D Systems, http://www.3dsystems.com.
93 Carbon, http://carbon3d.com.
94 Gizmo 3D Printers, http://www.gizmo3dprinters.com.au.
95 New Pro, http://newpro3d.com.
96 V. Chan, P. Zorlutuna, J. H. Jeong, H. Kong and R. Bashir, *Lab Chip*, 2010, **10**, 2062–2070.
97 V. Chan, J. H. Jeong, P. Bajaj, M. Collens, T. Saif, H. Kong and R. Bashir, *Lab Chip*, 2012, **12**, 88–98.
98 L.-H. Han, G. Mapili, S. Chen and K. Roy, *J. Manuf. Sci. Eng.*, 2008, **130**, 021005.
99 L.-H. Han, S. Suri, C. E. Schmidt and S. Chen, *Biomed. Microdevices*, 2010, **12**, 721–725.
100 G. Mapili, Y. Lu, S. Chen and K. Roy, *J. Biomed. Mater. Res., Part B*, 2005, **75**, 414–424.
101 S. P. Grogan, P. H. Chung, P. Soman, P. Chen, M. K. Lotz, S. Chen and D. D. D'Lima, *Acta Biomater.*, 2013, **9**, 7218–7226.
102 P. Soman, P. H. Chung, A. P. Zhang and S. Chen, *Biotechnol. Bioeng.*, 2013, **110**, 3038–3047.
103 S. Suri, L.-H. Han, W. Zhang, A. Singh, S. Chen and C. E. Schmidt, *Biomed. Microdevices*, 2011, **13**, 983–993.
104 P. Zorlutuna, J. H. Jeong, H. Kong and R. Bashir, *Adv. Funct. Mater.*, 2011, **21**, 3642–3651.
105 S.-H. Lee, J. J. Moon and J. L. West, *Biomaterials*, 2008, **29**, 2962–2968.
106 S. J. Leigh, H. T. J. Gilbert, I. A. Barker, J. M. Becker, S. M. Richardson, J. A. Hoyland, J. A. Covington and A. P. Dove, *Biomacromolecules*, 2013, **14**, 186–192.
107 J. L. Connell, E. T. Ritschdorff, M. Whiteley and J. B. Shear, *Proc. Natl. Acad. Sci. U. S. A.*, 2013, **110**, 18380–18385.
108 C. Cvetkovic, R. Raman, V. Chan, B. J. Williams, M. Tolish, P. Bajaj, M. S. Sakar, H. H. Asada, M. T. A. Saif and R. Bashir, *Proc. Natl. Acad. Sci. U. S. A.*, 2014, **111**, 10125–10130.
109 R. D. Kamm and R. Bashir, *Ann. Biomed. Eng.*, 2013, **42**, 445–459.
110 A. Tourovskaia, X. Figueroa-Masot and A. Folch, *Lab Chip*, 2005, **5**, 14–19.
111 A. Tourovskaia, T. F. Kosar and A. Folch, *Biophys. J.*, 2006, **90**, 2192–2198.
112 F. Zhu, T. Friedrich, D. Nugegoda, J. Kaslin and D. Wlodkowic, *Biomicrofluidics*, 2015, **9**, 061103.
113 N. P. Macdonald, F. Zhu, C. J. Hall, J. Reboud, P. S. Crosier, E. E. Patton, D. Wlodkowic and J. M. Cooper, *Lab Chip*, 2016, **16**, 291–297.
114 K. Modjarrad and S. Ebnesajjad, *Handbook of Polymer Applications in Medicine and Medical Devices*, William Andrew Publishing, 2014.
115 F. Pati, J. Jang, D.-H. Ha, S. Won Kim, J.-W. Rhie, J.-H. Shim, D.-H. Kim and D.-W. Cho, *Nat. Commun.*, 2014, **5**, 3935.
116 M. Mizutani and T. Matsuda, *J. Biomed. Mater. Res.*, 2002, **61**, 53–60.
117 S. D. Gittard, P. R. Miller, R. D. Boehm, A. Ovsianikov, B. N. Chichkov, J. Heiser, J. Gordon, N. A. Monteiro-Riviere and R. J. Narayan, *Faraday Discuss.*, 2011, **149**, 171–245.

118 J. Stampfl, S. Baudis, C. Heller, R. Liska, A. Neumeister, R. Kling, A. Ostendorf and M. Spitzbart, *J. Micromech. Microeng.*, 2008, **18**, 125014.
119 A. Doraiswamy, C. Jin, R. J. Narayan, P. Mageswaran, P. Mente, R. Modi, R. Auyeung, D. B. Chrisey, A. Ovsianikov and B. Chichkov, *Acta Biomater.*, 2006, **2**, 267–275.
120 A. Ovsianikov, B. Chichkov and P. Mente, *Int. J. Appl. Ceram. Technol.*, 2007, **4**, 22–29.
121 S. D. Gittard, A. Ovsianikov, B. N. Chichkov, A. Doraiswamy and R. J. Narayan, *Expert Opin. Drug Delivery*, 2010, **7**, 513–533.
122 C. G. Williams, A. N. Malik, T. K. Kim, P. N. Manson and J. H. Elisseeff, *Biomaterials*, 2005, **26**, 1211–1218.
123 R. Liska, M. Schuster, R. Inführ, C. Turecek, C. Fritscher, B. Seidl, V. Schmidt, L. Kuna, A. Haase, F. Varga, H. Lichtenegger and J. Stampfl, *J. Coat. Technol. Res.*, 2007, **4**, 505–510.
124 M. Schuster, C. Turecek, B. Kaiser, J. Stampfl, R. Liska and F. Varga, *J. Macromol. Sci., Part A: Pure Appl. Chem.*, 2007, **44**, 547–557.
125 B. D. Fairbanks, M. P. Schwartz, C. N. Bowman and K. S. Anseth, *Biomaterials*, 2009, **30**, 6702–6707.
126 J. W. Choi, H. C. Kim and R. Wicker, *J. Mater. Process. Technol.*, 2011, **211**(3), 318–328.
127 C. Zhou, Y. Chen, Z. Yang and B. Khoshnevis, *Rapid Prototyp. J.*, 2013, **19**, 153–165.
128 X. Zhang, X. N. Jiang and C. Sun, *Sens. Actuators, A*, 1999, **77**, 149–156.
129 J. W. Lee, I. H. Lee and D.-W. Cho, *Microelectron. Eng.*, 2006, **83**, 1253–1256.
130 P. Amend, O. Hentschel, C. Scheitler, M. Baum, J. Heberle, S. Roth and M. Schmidt, *J. Laser Micro/Nanoeng.*, 2013, **8**, 276–286.
131 X. Wang, X. Cai, Q. Guo, T. Zhang, B. Kobe and J. Yang, *Chem. Commun.*, 2013, **49**, 10064–10066.
132 J. Zhou, D. A. Khodakov, A. V. Ellis and N. H. Voelcker, *Electrophoresis*, 2012, **33**, 89–104.
133 K. Ohtani, M. Tsuchiya, H. Sugiyama, T. Katakura, M. Hayakawa and T. Kanai, *J. Oleo Sci.*, 2014, **63**, 93–96.
134 T. Kanai, K. Ohtani, M. Fukuyama, T. Katakura and M. Hayakawa, *Polym. J.*, 2011, **43**, 987–990.
135 M. Li and D. P. Kim, *Lab Chip*, 2011, **11**, 1126–1131.
136 E. Wilhelm, C. Neumann, K. Sachsenheimer, T. Schmitt, K. Länge and B. E. Rapp, *Lab Chip*, 2013, **13**, 2268–2271.
137 E. Wilhelm, K. Deshpande, F. Kotz, D. Schild, N. Keller, S. Heissler, K. Sachsenheimer, K. Länge, C. Neumann and B. E. Rapp, *Lab Chip*, 2015, **15**, 1772–1782.
138 I. R. G. Ogilvie, V. J. Sieben, B. Cortese, M. C. Mowlem and H. Morgan, *Lab Chip*, 2011, **11**, 2455–2459.
139 W. H. Grover, M. G. von Muhlen and S. R. Manalis, *Lab Chip*, 2008, **8**, 913–918.
140 K. L. Beattie, W. G. Beattie, L. Meng, S. L. Turner, R. Coral-Vazquez, D. D. Smith, P. M. McIntyre and D. D. Dao, *Clin. Chem.*, 1995, **41**, 700–706.
141 P. K. Yuen, *Lab Chip*, 2008, **8**, 1374–1378.
142 P. K. Yuen, J. T. Bliss, C. C. Thompson and R. C. Peterson, *Lab Chip*, 2009, **9**, 3303–3305.
143 K. C. Bhargava, B. Thompson and N. Malmstadt, *Proc. Natl. Acad. Sci. U. S. A.*, 2014, **111**, 15013–15018.
144 K. G. Lee, K. J. Park, S. Seok, S. Shin, D. H. Kim, J. Y. Park, Y. S. Heo, S. J. Lee and T. J. Lee, *RSC Adv.*, 2014, **4**, 32876–32880.
145 S. Tsuda, H. Jaffery, D. Doran, M. Hezwani, P. J. Robbins, M. Yoshida and L. Cronin, *PLoS One*, 2015, **10**, e0141640.
146 C. T. Riche, E. J. Roberts, M. Gupta, R. L. Brutchey and N. Malmstadt, *Nat. Commun.*, 2016, **7**, 10780.
147 G. A. Cooksey, C. G. Sip and A. Folch, *Lab Chip*, 2009, **9**, 417–426.
148 C. D. Robinson, J. M. Auchtung, J. Collins and R. A. Britton, *Infect. Immun.*, 2014, **82**, 2815–2825.
149 M. A. Unger, H. P. Chou, T. Thorsen, A. Scherer and S. R. Quake, *Science*, 2000, **288**, 113–116.
150 T. Thorsen, S. J. Maerkl and S. R. Quake, *Science*, 2002, **298**, 580–584.
151 A. K. Au, H. Lai, B. R. Utela and A. Folch, *Micromachines*, 2011, **2**, 179–220.
152 A. K. Au, N. Bhattacharjee, L. F. Horowitz, T. C. Chang and A. Folch, *Lab Chip*, 2015, **15**, 1934–1941.
153 C. I. Rogers, K. Qaderi, A. T. Woolley and G. P. Nordin, *Biomicrofluidics*, 2015, **9**, 016501.
154 H. Lai and A. Folch, *Lab Chip*, 2011, **11**, 336–342.
155 J. A. Weaver, J. Melin, D. Stark, S. R. Quake and M. A. Horowitz, *Nat. Phys.*, 2010, **6**, 218–223.
156 M. Rhee and M. A. Burns, *Lab Chip*, 2009, **9**, 3131–3143.
157 E. C. Jensen, W. H. Grover and R. A. Mathies, *J. Microelectromech. Syst.*, 2007, **16**, 1378–1385.
158 B. Mosadegh, C.-H. Kuo, Y.-C. Tung, Y.-S. Torisawa, T. Bersano-Begey, H. Tavana and S. Takayama, *Nat. Phys.*, 2010, **6**, 433–437.
159 P. N. Duncan, T. V. Nguyen and E. E. Hui, *Proc. Natl. Acad. Sci. U. S. A.*, 2013, **110**, 18104–18109.
160 N. S. G. K. Devaraju and M. A. Unger, *Lab Chip*, 2012, **12**, 4809–4815.
161 J. C. Licklider, *IRE Trans. Hum. Factors Electron.*, 1960, **1**, 4–11.
162 D. C. Engelbart, Augmenting human intellect: a conceptual framework (1962), in *Multimedia. From Wagner to Virtual Reality*, ed. P. Randall and K. Jordan, W. W. Norton & Company, New York, 2001, pp. 64–90.
163 Creative Commons, https://creativecommons.org.
164 T. Berners-Lee, googleblog.blogspot.com, 2014.
165 F. Gobba, *Int. Arch. Occup. Environ. Health*, 2006, **79**, 322–331.
166 G. M. Whitesides, *Nature*, 2006, **442**, 368–373.
167 P. Gould, *Mater. Today*, 2004, **7**, 48–52.

